RAPID EVALUATION OF NOTCH STRESS INTENSITY FACTORS USING THE PEAK STRESS METHOD: COMPARISON OF COMMERCIAL FINITE ELEMENT CODES FOR A RANGE OF MESH

RAPID EVALUATION OF NOTCH STRESS INTENSITY FACTORS USING THE PEAK STRESS METHOD: COMPARISON OF COMMERCIAL FINITE ELEMENT CODES FOR A RANGE OF MESH PATTERNS

G. Meneghetti[1*], A. Campagnolo[1], M. Avalle[2], D. Castagnetti[3], M. Colussi[4], P. Corigliano[5], M. De Agostinis[6], E. Dragoni[3], V. Fontanari[7], F. Frendo[8], L. Goglio[9], G. Marannano[10], G. Marulo[8], F. Moroni[11], A. Pantano[10], A. Rebora[2], A. Scattina[9], A. Spaggiari[3], B. Zuccarello[10]

[1] Department of Industrial Engineering, University of Padova, Via Venezia, 1 – 35131 Padova (Italy)

[2] Department of Mechanical, Energy, Management and Transportation Engineering, University of Genova, Via all'Opera Pia, 15 - 16145 Genova (Italy)

[3] Department of Sciences and Methods for Engineering, University of Modena and Reggio Emilia, Via Amendola 2 - 42122 Reggio Emilia (Italy)

[4] Department of Management and Engineering, University of Padova, Stradella San Nicola 3 - 36100 Vicenza, (Italy)

[5] Engineering Department, University of Messina, Contrada di Dio - 98166 Sant'Agata, Messina (Italy)

[6] Department of Industrial Engineering, University of Bologna, Viale del Risorgimento, 2 – 40136 Bologna (Italy)

[7] Department of Industrial Engineering, University of Trento, Via Sommarive, 9 - 38123 Povo, Trento (Italy)

[8] Department of Civil and Industrial Engineering, University of Pisa, Largo L. Lazzarino 2 - 56122 Pisa (Italy)

[9] Department of Mechanical and Aerospace Engineering, Politecnico di Torino, Corso Duca degli Abruzzi, 24 - 10129 Torino (Italy)

[10] Department of Industrial and Digital Innovation, University of Palermo, Viale delle Scienze - 90128, Palermo (Italy)

[11] Department of Engineering and Architecture, University of Parma, Via G. P Usberti 181/A - 43124 Parma (Italy)

[*]Corresponding author: giovanni.meneghetti@unipd.it, tel. 0039 049 8276751, fax 0039 049 8276785

ABSTRACT

The Peak Stress Method (PSM) is an engineering, FE-oriented method to rapidly estimate the Notch Stress Intensity Factors (NSIFs) by using the singular linear elastic peak stresses calculated from coarse FE analyses. The average element size adopted to generate the mesh pattern can be chosen arbitrarily within a given range. The advantages of the PSM can be summarized as follows: (i) coarse meshes can be adopted, the required FE size being some orders of magnitude larger than that necessary to evaluate the NSIFs from the local stress distributions; (ii) only a single stress value is sufficient to estimate the NSIFs instead of a number of stress-distance numerical results.

Originally, the PSM has been calibrated under pure mode I and pure mode II loadings by means of Ansys FE software. In the present contribution, a Round Robin between ten Italian Universities has been carried out in order to calibrate the PSM with seven different commercial FE codes. To this aim, several 2D mode I and mode II problems have been analysed independently by the participants. The obtained results have been used to calibrate the PSM for given stress analysis conditions in terms of: (i) FE software, (ii) element type and element formulation, (iii) mesh pattern and (iv) criteria for stress extrapolation and principal stress analysis at FE nodes.

Keywords: Notch Stress Intensity Factor (NSIF), Peak Stress Method (PSM), Finite Element (FE) Analysis, Coarse Mesh.

NOMENCLATURE

a	characteristic size of the analysed sharp V-notch
d	average size of a finite element mesh
e_1, e_2	parameters for the evaluation of the averaged strain energy density (SED)
E	elastic modulus
f_{w1}, f_{w2}	weight parameters of the peak stresses
K_1, K_2	mode I and II notch stress intensity factors (NSIFs)
K_{FE}^{*}, K_{FE}^{**}	non-dimensional K_1 and K_2 relevant to the peak stress method (PSM)
R_0	radius of the control volume for the averaged SED evaluation
r, θ	polar coordinates
u_x, u_y	displacement components in the Cartesian frame of reference
$\overline{W}$	strain energy density averaged over the control volume
x, y	Cartesian coordinates

Symbols

2α	opening angle
Δ	range of the considered quantity
λ_1, λ_2	mode I and mode II eigenvalues in Williams' equation
ν	Poisson's ratio

$\sigma_{I,peak}$	singular, linear elastic maximum principal stress evaluated at a V-notch tip by FEM using the mesh according to the PSM
$\sigma_{eq,peak}$	linear elastic equivalent peak stress evaluated at a V-notch tip
$\sigma_{ij,c}^{(A)}$	centroidal stress component in element *A*
$\sigma_{ij,k}^{(A)}$	stress component, referred to node *k* of element *A*
$\sigma_{ij,k}$	stress component, referred to node *k*
σ_{nom}	applied nominal stress
$\sigma_{\theta\theta}$, $\tau_{r\theta}$	normal and shear stress components in the polar frame of reference
$\sigma_{yy,peak}$	singular, linear elastic, opening peak stress evaluated at a V-notch tip by FEM according to the PSM
$\tau_{II,peak}$,$\tau_{xy,peak}$	singular, linear elastic, sliding peak stress evaluated at the crack tip by FEM according to the PSM
$[\sigma]_k^{(A)}$	stress tensor, referred to node *k* of element *A*
$[\sigma]_k$	stress tensor, referred to node *k*

Abbreviations

FE	Finite element
FEM	Finite element method
NSIF	Notch stress intensity factor
PSM	Peak stress method
SED	Strain energy density
SIF	Stress intensity factor

1. INTRODUCTION

In plane problems, the local linear elastic stress fields close to the tip of sharp V-notches, like those shown in the welded joint of Fig. 1, can be expressed as functions of the relevant NSIFs, which quantify the magnitude of the asymptotic singular stress distributions, according to the original analysis performed by Williams[1] under mode I (opening) and mode II (sliding) stresses. The mode I and mode II NSIFs can be defined according to Gross and Mendelson[2] by means of Eqs. (1) and (2), respectively (see Fig. 1b).

$$K_1 = \sqrt{2\pi} \cdot \lim_{r \to 0} \left[\left(\sigma_{\theta\theta} \right)_{\theta=0} \cdot r^{1-\lambda_1} \right] \tag{1}$$

$$K_2 = \sqrt{2\pi} \cdot \lim_{r \to 0} \left[\left(\tau_{r\theta} \right)_{\theta=0} \cdot r^{1-\lambda_2} \right] \tag{2}$$

In previous expressions, λ_1 and λ_2 are the stress singularity exponents[1], which depend on the notch opening angle 2α, while the stress components $\sigma_{\theta\theta}$ and $\tau_{r\theta}$ are calculated along the notch bisector

line, identified by the angular coordinate θ=0 (see Fig. 1). Values of λ_1 and λ_2 for the notch opening angles considered in the present contribution are reported in Table 1.

Notch stress intensity factors (NSIFs) have proved to efficiently correlate the static strength of components made of brittle or quasi-brittle materials and weakened by sharp V-notches[3–9], as well as the medium and high-cycle fatigue strength of notched components made of structural materials[10,11]. Concerning welded joints, NSIFs have been used to analyse the fatigue strength both under uniaxial[12–17] and multiaxial cyclic loadings[18]. However, calculating the NSIFs by means of finite element (FE) analyses presents a major drawback in engineering problems, because definitions (1) and (2) need very refined FE meshes in order to evaluate the NSIFs. Finite elements as small as 10^{-5} mm have been adopted in a previous study[13]; in case of three-dimensional components, numerical analyses could be even more time-consuming.

Recently, a simplified and rapid technique, the so-called Peak Stress Method (PSM), has been proposed in order to speed up the numerical evaluation of the NSIFs thanks to FE models with coarse meshes, i.e. some orders of magnitude larger than that required to apply definitions (1) and (2). The PSM is based on the numerical procedure proposed by Nisitani and Teranishi[19,20] to rapidly estimate the mode I SIF of a crack emanating from an ellipsoidal cavity. The method has been theoretically justified and extended to estimate also the mode I NSIF of sharp and open V-notches[21,22], the mode II SIF of cracks[23] and also the mode III NSIF of open V-notches[24].

Essentially, the PSM rapidly estimates the NSIFs K_1 and K_2 (Eqs. (1) and (2)) from the singular, linear elastic, opening (mode I) and sliding (mode II) FE peak stresses $\sigma_{I,peak}$ and $\tau_{II,peak}$, respectively, which are calculated at the node located at the V-notch tip (see the example of Fig. 1). When performing the FE analysis according to the PSM using a given software package, the following parameters must have been previously calibrated:

- the *element type* and *formulation*;
- the FE *mesh pattern;*

- the criteria for *stress extrapolation* and *principal stress analysis at FE nodes*

In more detail, the expressions of the PSM are the following[21,23]:

$$K_1 \cong K_{FE}^{*} \cdot \sigma_{I,peak} \cdot d^{1-\lambda_1} \tag{3}$$

$$K_2 \cong K_{FE}^{**} \cdot \tau_{II,peak} \cdot d^{0.5} \tag{4}$$

In previous expressions, *d* is the so-called 'global element size' parameter, i.e. the average size of the finite elements adopted by the free mesh generation algorithm available in the numerical code, while K^{*}_{FE} and K^{**}_{FE} take into account all calibration parameters mentioned previously. Besides the much more coarse mesh, the PSM has an additional advantage, which is illustrated by Eqs (3) and (4) as compared to previous expressions (1) and (2): only the singular, linear elastic peak stresses evaluated at the V-notch tip is sufficient, instead of a number of *stress-distance* numerical results.

Previously, the PSM has been calibrated by using the Ansys code and the following non-dimensional NSIFs have been obtained: $K^{*}_{FE} \cong 1.38$ and $K^{**}_{FE} \cong 3.38$. Such values are valid under the following conditions[21,23]:

- element types available in Ansys element library:
  - two-dimensional, 4-node quadrilateral finite elements with linear shape functions (PLANE 42 or alternatively PLANE 182 with K-option 1 set to 3, i.e. '*simple enhanced strain*' formulation activated);
  - three-dimensional, eight-node brick elements (SOLID 45 or equivalently SOLID 185 with K-option 2 set to 3, i.e. '*simple enhanced strain*' option activated);
  - two-dimensional, harmonic, 4-node linear quadrilateral elements, to analyse axis-symmetric components subjected to external loads that can be expressed according to a Fourier series expansion (PLANE 25).
- the FE mesh pattern close to the notch or crack tip must be that reported in Fig. 2 (see also[21,23]); in more detail, four elements share the node located at the notch tip if the notch

opening angle 2α is equal to or lower than 90°, while two elements share the node at notch tip when the notch opening angle is $2\alpha > 90°$. Figure 2 shows examples of such mesh patterns in case of symmetric FE models. It should be noted that the mesh patterns according to the PSM are automatically generated by the *free-mesh generation algorithm* of Ansys code, after having input the average FE size *d* by means of the 'global element size' command available in the software. There are not additional parameters or special settings to input in order to generate the mesh;

- Eq. (3) can be applied to sharp V-notches with an opening angle 2α between 0° and 135°; while calibration for mode II loading, Eq. (4), is restricted to the crack case ($2\alpha = 0$);
- the average element size *d* can be chosen arbitrarily, but within a range of applicability defined in the relevant literature[21,23]: for mode I loading (Eq. (3)), the mesh density ratio *a/d* must exceed 3 to obtain $K_{FE}^{*} = 1.38 \pm 3\%$; in case of mode II loading (Eq. (4)), more refined meshes are needed, the mesh density ratio *a/d* having to be greater than 14 to obtain $K_{FE}^{**} = 3.38 \pm 3\%$. In previous expressions *a* is the characteristic size of the analysed sharp V-notch, for example it is the notch depth in Fig. 2. More precisely, *a* is the minimum between the notch depth and the ligament size[25], indicated as *h* in the example of next Fig. 7, which will be commented later. In all geometries analysed in the present study, the characteristic size *a* resulted equal to the notch depth because a < h. There is only one exception in Table 3 (Fig. 7(c) with a = 15 mm and h = 10 mm) where h > a; however, to simplify the presentation of results, *a* was kept equal to the notch depth also in this case.

Any structural strength assessment criterion, which is based on NSIF parameters, can in principle be reformulated by using the PSM thanks to Eqs. (3) and (4). In the recent literature, the PSM has been coupled to the averaged strain energy density (SED) fatigue criterion to assess the fatigue strength of welded joints subjected to axial[23,25–27], torsion[24,28] and multiaxial[29,30] loading conditions. An example of such application will be given in the next paragraph.

To extend the use of the PSM in practical engineering problems, it is of paramount importance to calibrate the parameters K^{*}_{FE} (Eq. (3)) and K^{**}_{FE} (Eq. (4)) to commercial FE codes different from Ansys. Therefore, a Round Robin between some Italian Universities has been carried out in order to fill this gap, i.e. to check whether or not the parameters $K^{*}_{FE} \cong 1.38$ and $K^{**}_{FE} \cong 3.38$, previously calibrated by using Ansys, can be used also with other software packages. Possibly, they must be updated.

Accordingly, the PSM has been applied to sharp V-notches with different opening angles under pure mode I and cracks under pure mode II loadings by adopting different FE codes. After having calculated the peak stresses, the non-dimensional ratios K^{*}_{FE} and K^{**}_{FE} have been evaluated according to Eqs. (3) and (4), but now expressed in the following fashion:

$$K^{*}_{FE} \cong \frac{K_1}{\sigma_{I,peak} \cdot d^{1-\lambda_1}} \tag{5}$$

$$K^{**}_{FE} \cong \frac{K_2}{\tau_{II,peak} \cdot d^{0.5}} \tag{6}$$

Different commercial FE software packages have been used and for each of them calibration has been performed for fixed stress analysis conditions in terms of: (i) element type and element formulation, (ii) mesh pattern and (iii) criteria for stress extrapolation and principal stress analysis at FE nodes.

2. A PRACTICAL EXAMPLE: THE PSM APPLIED TO FATIGUE ASSESSMENT OF A WELDED JOINT

To illustrate the PSM in practical design situations, the fatigue strength assessment of conventional arc-welded joints made of structural steel is reported below. Load-carrying cruciform welded steel joints are considered (see the geometry in Fig. 3), which were fatigue tested by Ouchida e

Nishioka[31] under axial loading. The detailed analysis according to the PSM is reported in[26], to which the reader is referred. Only the main steps of the analysis are reported here.

The strain energy density (SED) averaged over a structural volume of radius R_0 surrounding the weld root or the weld toe (see Fig. 3), as proposed by Lazzarin and co-workers[7,17], is adopted as fatigue damage parameter. The averaged SED under mode I+II loading can be expressed in closed-form as a function of the relevant NSIFs according to Eq. (7).

$$\Delta\overline{W}=\frac{e_1}{E}\left(\frac{\Delta K_1}{R_0^{1-\lambda_1}}\right)^2+\frac{e_2}{E}\left(\frac{\Delta K_2}{R_0^{1-\lambda_2}}\right)^2 \tag{7}$$

where R_0 represents the control radius, ΔK_1 and ΔK_2 are the ranges of the NSIFs relevant to mode I and mode II, respectively, E is the Young's modulus, while e_1 and e_2 are known parameters depending on the notch opening angle 2α and the Poisson's ratio ν[7,17]. The size of the structural volume was calibrated on experimental fatigue test data and resulted R_0 = 0.28 mm for welded joints made of structural steel[17].

Taking advantage of the equality $W=\left(1-\nu^2\right)\cdot\sigma_{eq,peak}^2/2E$ valid under plane strain conditions, an equivalent peak stress, $\sigma_{eq,peak}$, can be derived as follow[26]:

$$\Delta\sigma_{eq,peak}=\sqrt{\frac{2}{1-\nu^2}\cdot\left[e_1\left(\frac{\Delta K_1}{R_0^{1-\lambda_1}}\right)^2+e_2\left(\frac{\Delta K_2}{R_0^{1-\lambda_2}}\right)^2\right]} \tag{8}$$

where e_1 and e_2 are known coefficients which depend on the notch opening angle 2α and the Poisson ratio; values relevant to the present paper are listed in Table 1. If ΔK_1 and ΔK_2 are evaluated directly at the weld toe and at the weld root by means of definitions, Eqs. (1) and (2), the mesh density must be very refined, as reported in Fig. 4. After applying definition (1), the mode I NSIFs were determined at the toe and root resulting in $\Delta K_{1,toe}$ = 3.40 MPa $mm^{0.326}$ and $\Delta K_{1,root}$ = 2.95 MPa $mm^{0.5}$, respectively, while mode II is not singular at weld toe and it is negligible at weld

root in this case ($\Delta K_{2,root} \approx 0$). It is worth noting that Fig. 4 reports the nodal stresses, therefore the minimum element size of 10^{-5} adopted in the FE simulation can be appreciated.

By using the PSM-based relationships (Eqs. (3) and (4)), Eq. (8) can be rewritten as a function of the singular, linear elastic FE peak stresses $\sigma_{I,peak}$ and $\tau_{II,peak}$[23]:

$$\Delta\sigma_{eq,peak}=\sqrt{f_{w1}^2 \cdot \Delta\sigma_{I,peak}^2 + f_{w2}^2 \cdot \Delta\tau_{II,peak}^2} \quad (9)$$

All parameter appearing in Eqs. (3), (4) and (8) are included in coefficients f_{w1} and f_{w2}, whose expression has been reported in the literature[23].

The peak stresses were calculated by using the FE mesh reported in Figure 5, according to the following steps:

- A 2D FE analysis was performed under plane strain conditions by adopting 4 node quadrilateral elements (PLANE 182 of Ansys element library, with K-option 1 set to 3, i.e. '*simple enhanced strain*' formulation activated)
- The mesh density ratio *a*/*d* was established as follows: *a* is the pre-crack length at the root side, so that the maximum FE size *d* is equal to *a*/3 = 3.5/3 → ≈ 1 mm is appropriate to apply Eq. (9); at the toe side, *a* is half the main plate thickness, i.e. *a* = 8 mm, therefore the maximum FE size is 8/3 = 2.66. In conclusion d = 1 mm is appropriate both at the root and at the toe side;
- The *free-mesh* pattern, see Fig. 5a was generated by setting a 'global element size' parameter *d* = 1 mm in the free mesh generation algorithm;
- The maximum principal stress $\Delta\sigma_{I,peak}$ was evaluated at the FE nodes located at the weld toe and root;
- Figure 5b shows the results according to PSM:
    - weld toe side: $\Delta\sigma_{eq,peak} \cong f_{w1} \cdot \Delta\sigma_{I,peak} = 1.064 \cdot 2.389 = 2.54$ MPa
    - weld root side: $\Delta\sigma_{eq,peak} \cong f_{w1} \cdot \Delta\sigma_{I,peak} = 1.410 \cdot 2.178 = 3.07$ MPa

As a conclusion, according to the PSM, the weld root is more critical than the weld toe, since $\Delta\sigma_{eq,peak}$ is higher at the root (3.07 MPa) than at the toe (2.54 MPa). This is in agreement with the fatigue crack initiation point experimentally observed by Ouchida e Nishioka[31]. Subsequently, the original experimental data have been reconverted in terms of equivalent peak stress evaluated at the weld root by means of Eq. (9). Finally, Figure 6 shows the comparison between the experimental results and the fatigue design scatter band previously calibrated in[26]. A good agreement between theoretical estimations and experimental results can be observed.

3. PARTICIPANTS AND FE CODES INVOLVED IN THE ROUND ROBIN

The participants and the FE codes involved in the Round Robin are listed in Table 2. Ten Universities took part to the project and seven commercial FE codes were calibrated.

Table 2 shows that Optistruct and Ls-Dyna were used to solve the numerical models, while Hypermesh and Hyperview were used as pre-processor and post-processor codes, respectively.

4. GEOMETRIES, MATERIAL AND FE MESH PATTERNS

A number of two dimensional geometries subjected to mode I or mode II loading conditions have been analysed by using the different FE codes. Geometries involved cracks as well as pointed V-notches and not necessarily reproduce welded joint geometries, because of the general validity of expressions (5) and (6) to be calibrated. Geometries, material properties, boundary conditions and FE type were obviously the same in all FE codes involved in the Round Robin. Conversely, as far as possible, specific options concerning element formulation, free mesh generation algorithms, stiffness matrix inversion algorithms, stress extrapolation and stress averaging rules at FE nodes have been set to *default options* in each software. Sometimes, with the sole aim to investigate the

reasons for different results obtained, the FE mesh pattern generated with a given software has been imported into another software, so that the results could be compared for precisely the same adopted mesh. All details concerning the analyses performed and the obtained results are given in the following.

4.1 2D problems (plane strain), mode I loading, $0° \le 2\alpha \le 135°$

Different geometries subjected to pure mode I as reported in Fig. 7 have been considered. All these case studies are the same adopted in the original calibration of the PSM under mode I loading which was performed by using Ansys FE code[21]. In particular, they consist of the following geometries: a crack located at the U-notch tip (Fig. 7(a)); a crack at the free surface of a finite-width plate (Fig. 7(b)); a plate with lateral open V-notches (Fig. 7(c)) and, finally, a typical full-penetration cruciform welded joint with a weld toe angle equal to 135° (Fig. 7(d)). The material is a structural steel with Young's modulus E = 206000 MPa and Poisson's ratio $\nu = 0.3$.

To calculate the peak stress values, linear elastic static analyses under plain strain conditions have been carried out and a FE pattern of four-node linear quadrilateral elements has been used as shown in the examples of Fig. 8, which refers to Ansys software. Only a quarter of each model has been analysed by taking advantage of the double symmetry condition. The free mesh generation algorithm was run in each software after setting the average element size d to adopt. The mesh density ratio a/d was varied in a wide range by considering either a variation of the notch/crack size a or a variation of the FE size d, as reported in Table 3.

All generated meshes were checked to assure that the FE pattern at the notch or crack tip was of the type shown in Fig. 2. If the mesh pattern generated by the free mesh generator was not the standard one reported in Fig. 2 (in a symmetric model one element was sometimes obtained at the notch tip when $2\alpha = 90°$, instead of two, or two elements were sometimes obtained when $2\alpha = 135°$, instead of one), then mesh generation was repeated by changing slightly the average element size d up to

10% of the nominal values reported in Table 3 until the standard mesh was obtained. In these cases, the actual *d* value has been adopted to calculate the ratio *a/d* and K^*_{FE} (Eq. 5). Fig. 8 highlights that there has not been any division of the area of the model into sub-areas. The external load has been applied as a nominal gross-section stress equal to 1 MPa.

After solving the FE model, the peak value of the maximum principal stress $\sigma_{I,peak}$ was taken at the FE node located at the V-notch tip (see Fig. 8). Stress averaging at FE nodes was activated in each FE code, so that only a single stress value for $\sigma_{I,peak}$ has been obtained per node by averaging the nodal stresses from all elements that share the node. To this end, the default options of each FE code have been used, whenever possible, as it will be explained in detail in the following.

The exact mode I NSIFs K_1, to input in Eq. (5), were derived by using Ansys software and by applying definition (1) to the stress-distance numerical results obtained from very refined FE mesh patterns (the size of the smallest element close to the V-notch tip was of the order of 10^{-5} mm).

4.2 2D problems (plane strain), mode II loading, $2\alpha = 0°$

A crack ($2\alpha = 0°$) centred in a plate having the geometry reported in Fig. 9 and subjected to pure mode II loading was considered. The case study has been taken from the original calibration of the PSM under mode II loading conditions for Ansys FE code[23]. The considered material is a structural steel with Young's modulus E = 206000 MPa and Poisson's ratio $\nu = 0.3$.

The peak stresses were calculated by means of linear elastic static analyses under plain strain conditions and a pattern of four-node linear quadrilateral elements as shown in the example of Fig. 10. The mesh density ratio *a/d* was varied in a wide range from 1 to 200 as reported in Table 4. Only a quarter of the cracked plate has been analysed by taking advantage of the double anti-symmetry boundary conditions (see Fig. 10).

The external load has been applied to the FE model by means of displacements $u_x=u_y=1.262\cdot10^{-3}$ mm at the plate free edges. Such displacements translate into a nominal gross shear stress equal to 1

MPa in absence of the crack. After solving the FE model, the peak value of the (mode II) shear stress $\tau_{xy,peak} = \tau_{II,peak}$ has been taken at the node located at the crack tip (see Fig. 10). Stress averaging at FE nodes has been activated as explained for mode I analyses. Again, the exact mode II SIFs K_2 to input in Eq. (6), were calculated by using Ansys and by applying definition (2) to the stress-distance numerical results obtained from very refined FE mesh patterns (the size of the smallest element close to the crack tip was of the order of 10^{-5} mm).

5. DETAILS OF MESH GENERATION SETTINGS

It has been mentioned that two-dimensional, four-node, linear quadrilateral elements under plane strain hypothesis were adopted in the FE analyses. The element was integrated by using 2x2 Gauss points. After selecting the proper element type, the average element size *d*, which was input by the FE analyst, has been the sole parameter used in order to drive the automatic free mesh generation algorithm. In the following, details concerning element type/options along with the adopted mesh generation settings are reported for each FE code:

- ***Ansys***

  Element type: Solid → Quad 4-node (PLANE 42 or PLANE 182)

  Element options: Plane strain, Simple enhanced strain (only for PLANE 182)

  Element size: Size Cntrls → Manual Size → Global → Size = *d*

  Mesh generation: Mesh → Areas → Free

- ***Abaqus***

  Element type: Standard → linear → Quad

  Element options: Plane strain, Incompatible modes (CPE4I)

  Element size: Global Seeds → Sizing Cntrls → Approximate global size = *d*

  Mesh generation: Mesh Cntrls → Free → Advancing front → "Use mapped meshing where appropriate" MUST BE INACTIVE; Mesh Part Instance → Ok

- ***Straus 7***

  Element type: linear 4-node quadrilateral plate (QUAD4)

  Element options: Plane strain

  Element size: Automeshing → Surface mesh → Sizes → Maximum edge length = *d*

  Mesh generation: Automeshing → Surface mesh → Mesh

- ***MSC Patran/Nastran***

  Element type: 2D Solid (CQUAD4)

  Element options: Plane strain, Standard formulation

  Element size: Mesh → Surface → Global Edge Length → Value = *d*

  Mesh generation: Mesh → Surface → Elem Shape → Quad; Mesher → Paver; Topology → Quad4

- ***Lusas***

  Element type: 2D continuum element with enhanced strains (QPN4M)

  Element options: Plane strain, Quadrilateral, Linear interpolation

  Element size: Mesh → Surface Mesh → Irregular mesh → Element size = *d*

  Mesh generation: Mesh → Surface Mesh

- ***Hypermesh/Optistruct/Hyperview***

  Element type: Shell 4-node (*Hypermesh*), CQUAD4 (*Optistruct*)

  Element options: MID2 = -1 (plane strain), MID3 = blank (*Optistruct*)

  Element size: Mesh → Surfs → Size and bias → Element size = *d* (*Hypermesh*)

  Mesh generation: Mesh → Surfs → Mesh type → quads; mesh (*Hypermesh*)

- ***Hypermesh/Ls-Dyna/Hyperview***

  Element type: Shell 4-node (*Hypermesh*)

  Element options: Element formulation 13 (Plane strain x-y plane) (*LS-Dyna*)

  Element size: Mesh → Surfs → Size and bias → Element size = *d (Hypermesh)*

Mesh generation: Mesh → Surfs → Mesh type → quads; mesh (*Hypermesh*)

6. RESULTS OF FE ANALYSES

The results obtained from the participants to the Round Robin are reported in Figs. 11a-g and 12 for mode I and mode II problems, respectively. The figures show the non-dimensional ratios K^{*}_{FE} and K^{**}_{FE}, defined in Eqs. (5) and (6), respectively, as a function of the mesh density ratio *a/d*. Results shown in Figs. 11a-g and 12 have been obtained with the *default options* of the post-processing environment, which are listed in the following for the sake of clarity:

- ***Ansys***

  Options for outputs: Principal stress calcs → from components (or equivalently AVPRIN = 0)

- ***Abaqus***

  Result options: Averaging → Compute order → Compute scalars before averaging → Averaging threshold = 100 %

- ***Straus 7***

  Node average: Always

- ***MSC Patran/Nastran***

  Averaging definition: Method → Derive/Average

- ***Lusas***

  Properties: Value results → Location → Averaged nodal

- ***Hypermesh/Optistruct/Hyperview***

  Averaging method: Simple

- ***Hypermesh/Ls-Dyna/Hyperview***

  Averaging method: Simple

Dealing with mode I loading, it can be observed from Figs. 11b-e that the majority of the considered FE codes, i.e. Abaqus, Straus 7, MSC Patran/Nastran and Lusas, present the same parameter $K^*_{FE} \cong 1.38$ that had been previously calibrated in Ansys[21] and it is reported in Fig. 11a. It should be noted that for all FE codes convergence is achieved for a mesh density ratio $a/d \geq 3$, such value being consistent once more with the original calibration[21]. A slightly greater scatter band of ±5% should instead be accepted, as compared to ref.[21] where ±3% was found.

On the other hand, Figures 11f,g show that the FE packages Hypermesh/Optistruct/Hyperview and Hypermesh/Ls-Dyna/Hyperview present a different calibration constant, i.e. $K^*_{FE} \cong 1.84$. This peculiar behaviour depends on stress extrapolation rules at FE nodes and will be analysed later on. Moreover, the scatter ±8% (see Figs. 11f,g) is higher as compared to ±5% obtained with the other FE codes (see Figs. 11a,e).

Dealing with mode II loading, Fig. 12 reports the results and shows that all considered FE codes converge to $K^{**}_{FE} \cong 3.38 \pm 3\%$, i.e. the values calibrated previously for Ansys software[23]. Convergence is achieved for a mesh density ratio $a/d \geq 14$, which is consistent with the original calibration[23].

All results reported in Figs 11 and 12 are summarized in Table 5, which reports the non-dimensional ratios K^*_{FE} and K^{**}_{FE} to use in Eqs. (3), (4) and (9) and the minimum mesh density ratio a/d for all considered FE codes.

7. DISCUSSION

In the previous paragraph, it has been observed that under mode I loading there are some discrepancies among the results delivered by the different FE codes. As a major discrepancy, Fig. 11 and Table 5 show that Hypermesh/Optistruct/Hyperview and Hypermesh/Ls-Dyna/Hyperview converge to $K^*_{FE} = 1.84$, while all other FE codes converge to $K^*_{FE} = 1.38$. Minor differences in results delivered by the different FE codes also exist but they are taken up by the scatter bands.

Such discrepancies have been explained by examining the different procedures for stress extrapolation and principal stress analysis at FE nodes, mesh patterns adopted by the different FE codes and numerical integration schemes. Detailed explanations are given in the following.

7.1 Stress extrapolation at FE nodes

FE codes compute results at the integration (or Gauss) points. Afterwards, results can be computed at nodal or centroidal locations, based on the element shape functions. Once the nodal or centroidal stress in the element is obtained, it is possible to calculate the stress at a node shared by more than one element according to two different procedures, which are sketched in Fig. 13:

(a) The nodal stresses in the element ($\sigma_{ij,k}^{(A)}$ and $\sigma_{ij,k}^{(B)}$ in Fig. 13a) are extrapolated from the stresses at the integration points. Afterwards, the stress at the shared node ($\sigma_{ij,k}$ in Fig. 13a) is calculated by averaging the nodal stresses per element according to expression:

$$\sigma_{ij,k} = \frac{\sigma_{ij,k}^{(A)} + \sigma_{ij,k}^{(B)}}{2} \tag{10}$$

(b) The centroidal stresses in the element ($\sigma_{ij,c}^{(A)}$ and $\sigma_{ij,c}^{(B)}$ in Fig. 13b) are interpolated from the stresses at the integration points and are attributed to the shared node ($\sigma_{ij,k}$ in Fig. 13b). Then, the stress at the shared node is calculated according to the expression:

$$\sigma_{ij,k} = \frac{\sigma_{ij,c}^{(A)} + \sigma_{ij,c}^{(B)}}{2} \tag{11}$$

It should be noted that stress extrapolation at nodes according to Fig. 13a and Eq. (10) is carried out by most of the considered FE codes, i.e. Ansys, Abaqus, Straus 7, MSC Patran/Nastran and Lusas. On the other hand, the postprocessor Hyperview allows to adopt either Eq. (10) or Eq. (11); however both Optistruct and Ls-Dyna do not calculate the nodal stresses in the element, so that Hyperview can extrapolate stress at nodes only according to Fig. 13b and Eq. (11). This is the

reason why K^*_{FE} obtained with Optistruct and Ls-Dyna (Figs 11f-g) is different from that obtained with the other FE codes (Figs 11a-e).

To support this conclusion, calibration under mode I has been repeated by adopting Ansys FE software, but now forcing the use of Eq. (11) (see Fig. 13b) to calculate the nodal stresses. The obtained results are reported in Fig. 14, where it is seen that under these conditions Ansys converges to the same value $K^*_{FE} \cong 1.84$ reported in Figs. 11f,g for Hypermesh/Optistruct/Hyperview and Hypermesh/Ls-Dyna/Hyperview. To mimic these software packages with Ansys as accurately as possible, the averaging option (b) reported in next Table 6, and the full integration option, as reported in next Table 9, were adopted. This point will be clarified when commenting on the relevant Tables.

7.2 Principal stress averaging

Whatever the nodal stress evaluation technique (either Eq. (10) or Eq. (11)), the principal stresses at a node shared by more than one element can be calculated by adopting one of the following averaging procedures (see also Fig. 15):

(a) The nodal stress tensors per element ($[\sigma]_k^{(A)}$ and $[\sigma]_k^{(B)}$ in Fig. 15a) are averaged at the shared node ($[\sigma]_k$ in Fig. 15a) and then nodal principal stresses are calculated ($\sigma_{11,k}$ is the maximum principal stress in Fig. 15a).

(b) The nodal principal stresses per element ($\sigma_{11,k}^{(A)}$ and $\sigma_{11,k}^{(B)}$ in Fig. 15b) are calculated from the relevant nodal stress tensor per element ($[\sigma]_k^{(A)}$ and $[\sigma]_k^{(B)}$ in Fig. 15b) and then nodal principal stresses per element are averaged at the shared node ($\sigma_{11,k}$ in Fig. 15b).

Table 6 reports the nomenclature adopted by each FE code to define options (a) and (b) for principal stress averaging. The *default option* is also indicated in the table and it has been adopted to calibrate the PSM. It should be noted that option (a) is the default for Ansys and Lusas, while

option (b) is the default for all other FE codes. This is the reason why averaging option (b) was adopted in Ansys to prepare Fig. 14. The different principal stress averaging techniques are one of the reasons for small discrepancies among the results provided by the FE codes: however, such differences are taken up by the scatter band reported in previous Fig. 11.

7.3 FE mesh pattern

Different mesh patterns were generated by the different FE codes for the same analysed geometry and adopted global element size d. However, it is worth noting that such differences did not involve the number of elements sharing the node at the V-notch tip, because in all cases the standard pattern prescribed in Fig. 2 were obtained, as pointed out previously.

The influence of different mesh patterns has been investigated by considering a case study consisting of the mode I problem of Fig. 7c with notch depth a = 15 mm, notch opening angle $2\alpha = 90°$ and global element size d = 1 mm. The FE meshes generated by a selection of FE codes, namely Ansys, Abaqus and MSC Patran/Nastran, are reported in Table 7 along with the results in terms of peak stresses evaluated at the notch tip. Again, stress values obtained by adopting the *default options* (which have been employed here to calibrate the PSM) are highlighted.

Table 7 allows to quantify the effect of different mesh patterns (in terms of shape and arrangement of the elements) on the peak stress values for the same principal stress averaging option. However, in the context of the present Round Robin, comparison among the three FE codes should not be made for the same averaging option, but rather for the default option of each FE code. It is seen that the differences among the calculated stresses (6.309, 6.093 and 6.386 in Ansys, Abaqus and MSC Patran/Nastran, respectively) is reduced and it is included in the scatter bands reported in Fig. 11.

7.4 Numerical integration scheme

Each FE software provides different integration scheme options for the same element type, which typically cover full and reduced integrations, but, optionally, include also some enhanced formulations that allow to avoid numerical errors, associated to shear locking, hourglass effect and volumetric locking.

In order to investigate the effect of different integration schemes, the 2D mode I problem of Fig. 7c with notch depth a = 15 mm, notch opening angle $2\alpha = 90°$ and global element size d = 1 mm was considered again as a case study. To exclude the effect of the mesh pattern, a FE mesh has been generated in Ansys by using the free mesh generation algorithm (see Fig. 16) and afterwards it has been imported into all FE codes involved in the present Round Robin. By doing so, identical mesh patterns have been used with different FE codes. All available options associated to a 2x2 Gauss point integration scheme have been adopted in each FE code.

The results in terms of peak stresses evaluated at the notch tip are reported in Tables 8 and 9, where *default options* are highlighted. Table 8 lists the results calculated with FE codes which employ Eq. (10) to evaluate nodal stresses, while Table 9 reports the stress values calculated by FE codes which adopt Eq. (11). In Table 9 results from Ansys and Straus 7 have been included for comparison purposes: however, all calculations were made by hand, because Ansys and Straus 7 do not implement stress averaging at FE nodes when stresses at element centroids are used. Table 8 shows the perfect match of the fully integrated elements between Ansys and Abaqus. Moreover, the simple enhanced strain formulation in Ansys, adopted to perform the original calibration of the PSM[21], fully agrees with the standard formulation of MSC Patran/Nastran. Table 9 shows the excellent agreement of Hypermesh/Optistruct/Hyperview and Hypermesh/Ls-Dyna/Hyperview software packages with the fully integrated plane elements of Ansys. This is the reason why full integration was adopted in Ansys to compile previous Fig. 14.

The different integration scheme options adopted by the different FE packages is a further source of scatter of results; however, all of them are taken up by the proposed scatter bands.

It is interesting to note that some commercial FE codes, other than those considered here, provide the full integration scheme as the *default* setting or even as the sole option; therefore calibrating the PSM by adopting this formulation might be useful. To this aim, mode I analyses have been repeated by adopting Ansys and Abaqus FE codes, by adopting the full integration scheme and by calculating results according to the averaging option (b) (see Fig. 15b). The results are reported in Fig. 17 and it is seen that both FE codes converge to the value $K^*_{FE} \cong 1.55$. However, a slightly greater scatter band of ±8% should be accepted for Abaqus (Fig. 17b) as compared to ±5% valid for Ansys (Fig. 17a). This difference can be explained on the basis of the different local mesh patterns generated by Ansys and Abaqus FE codes: two examples are highlighted inside Figs. 17a,b, which show that the free mesh generation algorithm of Ansys provides very similar mesh patterns for the two cases; differently, Abaqus provides quite different mesh patterns for the same cases, giving rise to a slightly increased scattering of results. Finally, it should be noted that for both Ansys and Abaqus FE codes, the convergence is guaranteed for a mesh density ratio $a/d > 3$, such value being consistent with previous calibrations reported in Fig. 11.

8. CONCLUSIONS

A Round Robin has been carried out in order to calibrate the Peak Stress Method (PSM) to rapidly estimate the linear elastic Notch Stress Intensity Factor (NSIF) parameters relevant to mode I and mode II loadings with different commercial FE codes and a range of coarse mesh patterns. Essentially, the PSM is a simplified, FE-oriented numerical technique originally calibrated using Ansys software, which takes the singular, linear elastic peak stresses calculated at the point of singularity with coarse FE meshes to estimate the mode I NSIF and the mode II SIF. Two

calibration constants are needed, namely K^*_{FE} (Eq. (3)) and K^{**}_{FE} (Eq. (4)), respectively, which have been calibrated in this paper for some FE software packages, other than Ansys. The following conclusions can be drawn from the present study:

- Dealing with mode I loading, FE codes that extrapolate nodal stresses on the basis of nodal stresses per element, namely Ansys, Abaqus, Straus 7, MSC Patran/Nastran and Lusas, present the same calibration constant, i.e. $K^*_{FE} \cong 1.38$, as originally found for Ansys software. FE results fall within a scatter band of ±5% when the mesh density ratio *a/d* is equal to or greater than 3. On the other hand, FE codes that extrapolate nodal stresses on the basis of centroidal stresses, namely Hypermesh/Optistruct/Hyperview and Hypermesh/Ls-Dyna/Hyperview, present a different value, i.e. $K^*_{FE} \cong 1.84$. In this case, FE results were seen to fall in a slightly wider scatter band of ±8%, when the mesh density ratio is again $a/d \geq 3$.
- Dealing with mode II loading, all FE codes involved in the Round Robin present the same calibration constant independently of the nodal stress extrapolation procedure, i.e. $K^{**}_{FE} \cong 3.38$ with a scatter band of ±3% for a mesh density ratio $a/d \geq 14$. All these results are consistent with the original calibration of Ansys software.
- The effects of principal stress averaging options, mesh patterns and element formulation settings have been investigated. In summary, when adopting the *default options* of each software, the influence of all previous analysis features are taken up by the scatter bands of ±5% or ±8% defined for the calibration constant K^*_{FE} and ±3% valid for K^{**}_{FE}.
- As a side result, Ansys and Abaqus were run also by setting fully integrated, four-node elements and principal stress averaging from principals. These settings are the default ones for existing FE packages other than those analysed in the present work. The result obtained

was $K^*_{FE} \cong 1.55$ with a scatter band of ±5% for Ansys and of ±8% for Abaqus, provided that the mesh density ratio *a/d* is equal to or greater than 3.

ACKNOWLEDGEMENTS

The Round Robin was conceived and conducted by the Working Group on "*Joining Techniques*" of the Italian Association for Stress Analysis (AIAS). The precious effort of all participants is gratefully acknowledged.

REFERENCES

1. Williams ML (1952). Stress singularities resulting from various boundary conditions in angular corners of plates in tension. *J Appl Mech*, 19, 526–528.
2. Gross B, Mendelson A (1972). Plane elastostatic analysis of V-notched plates. *Int. J. Fract. Mech.*, 8, 267–276.
3. Seweryn A (1994). Brittle fracture criterion for structures with sharp notches. *Eng. Fract. Mech.*, 47, 673–681.
4. Nui LS, Chehimi C, Pluvinage G (1994). Stress field near a large blunted tip V-notch and application of the concept of the critical notch stress intensity factor (NSIF) to the fracture toughness of very brittle materials. *Eng. Fract. Mech.*, 49, 325–335.
5. Fett T (1996). Failure of brittle materials near stress singularities. *Eng. Fract. Mech.*, 53, 511–518.
6. Dunn ML, Suwito W, Cunningham S, May CW (1997). Fracture initiation at sharp notches under mode I, mode II, and mild mixed mode loading. *Int. J. Fract.*, 84, 367–381.
7. Lazzarin P, Zambardi R (2001). A finite-volume-energy based approach to predict the static and fatigue behavior of components with sharp V-shaped notches. *Int. J. Fract.*, 112, 275–298.
8. Gómez FJ, Elices M (2003). A fracture criterion for sharp V-notched samples. *Int. J. Fract.*, 123, 163–175.
9. Planas J, Elices M, Guinea G., Gómez F., Cendón D., Arbilla I (2003). Generalizations and specializations of cohesive crack models. *Eng. Fract. Mech.*, 70, 1759–1776.
10. Kihara S, Yoshii A (1991). A Strength Evaluation Method of a Sharply Notched Structure by

a New Parameter, 'The Equivalent Stress Intensity Factor'. *JSME Int. journal. Ser. 1, Solid Mech. strength Mater.*, 34, 70–75.

11. Boukharouba T, Tamine T, Niu L, Chehimi C, Pluvinage G (1995). The use of notch stress intensity factor as a fatigue crack initiation parameter. *Eng. Fract. Mech.*, 52, 503–512.
12. Verreman Y, Nie B (1996). Early development of fatigue cracking at manual fillet welds. *Fatigue Fract. Eng. Mater. Struct.*, 19, 669–681.
13. Lazzarin P, Tovo R (1998). A notch intensity factor approach to the stress analysis of welds. *Fatigue Fract. Eng. Mater. Struct.*, 21, 1089–1103.
14. Lazzarin P, Livieri P (2001). Notch stress intensity factors and fatigue strength of aluminium and steel welded joints. *Int. J. Fatigue*, 23, 225–232.
15. Atzori B, Meneghetti G (2001). Fatigue strength of fillet welded structural steels: finite elements, strain gauges and reality. *Int. J. Fatigue*, 23, 713–721.
16. Lazzarin P, Lassen T, Livieri P (2003). A notch stress intensity approach applied to fatigue life predictions of welded joints with different local toe geometry. *Fatigue Fract. Eng. Mater. Struct.*, 26, 49–58.
17. Livieri P, Lazzarin P (2005). Fatigue strength of steel and aluminium welded joints based on generalised stress intensity factors and local strain energy values. *Int. J. Fract.*, 133, 247–276.
18. Lazzarin P, Sonsino CM, Zambardi R (2004). A notch stress intensity approach to assess the multiaxial fatigue strength of welded tube-to-flange joints subjected to combined loadings. *Fatigue Fract. Eng. Mater. Struct.*, 27, 127–140.
19. Nisitani H, Teranishi T (2001). K_I value of a circumferential crack emanating from an ellipsoidal cavity obtained by the crack tip stress method in FEM. In: Guagliano M, Aliabadi MH (eds) *Proceedings of the 2nd international conference on fracture and damage mechanics*, pp. 141–146.
20. Nisitani H, Teranishi T (2004). K_I of a circumferential crack emanating from an ellipsoidal cavity obtained by the crack tip stress method in FEM. *Eng. Fract. Mech.*, 71, 579–585.
21. Meneghetti G, Lazzarin P (2007). Significance of the elastic peak stress evaluated by FE analyses at the point of singularity of sharp V-notched components. *Fatigue Fract. Eng. Mater. Struct.*, 30, 95–106.
22. Meneghetti G, Guzzella C (2014). The peak stress method to estimate the mode I notch stress intensity factor in welded joints using three-dimensional finite element models. *Eng. Fract. Mech.*, 115, 154–171.

23. Meneghetti G (2012). The use of peak stresses for fatigue strength assessments of welded lap joints and cover plates with toe and root failures. *Eng. Fract. Mech.*, 89, 40–51.
24. Meneghetti G (2013). The peak stress method for fatigue strength assessment of tube-to-flange welded joints under torsion loading. *Weld. World*, 57, 265–275.
25. Meneghetti G, Campagnolo A, Berto F (2015). Fatigue strength assessment of partial and full-penetration steel and aluminium butt-welded joints according to the peak stress method. *Fatigue Fract. Eng. Mater. Struct.*, 38, 1419–1431.
26. Meneghetti G, Lazzarin P (2011). The Peak Stress Method for Fatigue Strength Assessment of welded joints with weld toe or weld root failures. *Weld. World*, 55, 22–29.
27. Meneghetti G, Guzzella C, Atzori B (2014). The peak stress method combined with 3D finite element models for fatigue assessment of toe and root cracking in steel welded joints subjected to axial or bending loading. *Fatigue Fract. Eng. Mater. Struct.*, 37, 722–739.
28. Meneghetti G, De Marchi A, Campagnolo A (2016). Assessment of root failures in tube-to-flange steel welded joints under torsional loading according to the Peak Stress Method. *Theor. Appl. Fract. Mech.*, 83, 19–30.
29. Meneghetti G, Campagnolo A, Rigon D (2017). Multiaxial fatigue strength assessment of welded joints using the Peak Stress Method – Part I: Approach and application to aluminium joints. *Int. J. Fatigue*, 101, 328–342.
30. Meneghetti G, Campagnolo A, Rigon D (2017). Multiaxial fatigue strength assessment of welded joints using the Peak Stress Method – Part II: Application to structural steel joints. *Int. J. Fatigue*, 101, 343–362.
31. Ouchida H, Nishioka A (1964). A study of fatigue strength of fi llet welded joints. In: *IIW Doc. XIII-338-64*.

RAPID EVALUATION OF NOTCH STRESS INTENSITY FACTORS USING THE PEAK STRESS METHOD: COMPARISON OF COMMERCIAL FINITE ELEMENT CODES FOR A RANGE OF MESH PATTERNS

G. Meneghetti[1*], A. Campagnolo[1], M. Avalle[2], D. Castagnetti[3], M. Colussi[4], P. Corigliano[5], M. De Agostinis[6], E. Dragoni[3], V. Fontanari[7], F. Frendo[8], L. Goglio[9], G. Marannano[10], G. Marulo[8], F. Moroni[11], A. Pantano[10], A. Rebora[2], A. Scattina[9], A. Spaggiari[3], B. Zuccarello[10]

[1] Department of Industrial Engineering, University of Padova, Via Venezia, 1 – 35131 Padova (Italy)

[2] Department of Mechanical, Energy, Management and Transportation Engineering, University of Genova, Via all'Opera Pia, 15 - 16145 Genova (Italy)

[3] Department of Sciences and Methods for Engineering, University of Modena and Reggio Emilia, Via Amendola 2 - 42122 Reggio Emilia (Italy)

[4] Department of Management and Engineering, University of Padova, Stradella San Nicola 3 - 36100 Vicenza, (Italy)

[5] Engineering Department, University of Messina, Contrada di Dio - 98166 Sant'Agata, Messina (Italy)

[6] Department of Industrial Engineering, University of Bologna, Viale del Risorgimento, 2 – 40136 Bologna (Italy)

[7] Department of Industrial Engineering, University of Trento, Via Sommarive, 9 - 38123 Povo, Trento (Italy)

[8] Department of Civil and Industrial Engineering, University of Pisa, Largo L. Lazzarino 2 - 56122 Pisa (Italy)

[9] Department of Mechanical and Aerospace Engineering, Politecnico di Torino, Corso Duca degli Abruzzi, 24 - 10129 Torino (Italy)

[10] Department of Industrial and Digital Innovation, University of Palermo, Viale delle Scienze - 90128, Palermo (Italy)

[11] Department of Engineering and Architecture, University of Parma, Via G. P Usberti 181/A - 43124 Parma (Italy)

[*]Corresponding author: giovanni.meneghetti@unipd.it, tel. 0039 049 8276751, fax 0039 049 8276785

CAPTIONS TO FIGURES AND TABLES

Figure 1: Sharp V-shaped notches in a welded joint (a) at the root ($2\alpha = 0°$) (b) and at the toe (2α typically equal to 135°) (c) sides. Definition of peak stresses $\sigma_{I,peak}$ and $\tau_{II,peak}$ evaluated at the weld toe and the weld root by means of a linear elastic finite element analysis.

Figure 2: Mesh patterns according to the PSM[21,23]. Symmetry boundary conditions have been applied to the FE model.

Figure 3: Geometry of the load-carrying steel weld joint tested in[31]. Control volumes for the averaged SED evaluation at the weld toe and the weld root sides.

Figure 4: Singular, linear elastic stress fields at the weld toe and the weld root, obtained from very refined FE mesh patterns (minimum FE size $d_{min} \approx 10^{-5}$ mm) and comparison with the asymptotic solutions based on the relevant NSIF. The nominal applied stress $\Delta\sigma_{nom}$ is equal to 1 MPa.

Figure 5: Application of the PSM to the fatigue strength assessment of a load-carrying arc-welded joint made of structural steel and tested in[31].

Figure 6: Fatigue assessment of load-carrying steel welded joints according to the PSM. Comparison between the fatigue design scatter band of the PSM[26] and experimental fatigue results from[31].

Figure 7: Geometries of 2D problems (plane strain) under mode I loading. Dimensions in [mm].

Figure 8: FE mesh patterns and boundary conditions applied into the FE analyses of 2D problems (plane strain) under mode I loading. Geometries are reported in Fig. 7. FE patterns shown in the figure have been generated by using Ansys.

Figure 9: Geometry of 2D problems (plane strain) under mode II loading. Dimensions in [mm].

Figure 10: FE mesh pattern and boundary conditions applied into the FE analyses of 2D problems (plane strain) under mode II loading. Geometry is reported in Fig. 9. The FE pattern shown in the figure has been generated by using Ansys.

Figure 11: Results of Round Robin for mode I loading: non-dimensional ratio K^{*}_{FE} for each FE code.

Figure 12: Results of Round Robin for mode II loading: non-dimensional ratio K^{**}_{FE} for all considered FE codes.

Figure 13: Stress extrapolation at the nodes based on (a) nodal stresses or (b) centroidal stresses.

Figure 14: Non-dimensional ratio K^{*}_{FE} for Ansys FE code. Results for mode I loading based on centroidal stresses (according to Fig. 13b).

Figure 15: Principal stress averaging options. (a) Principal stresses from average stress tensor. (b) Principal stresses from element principal stresses.

Figure 16: FE mesh pattern relevant to case 7c with a = 15 mm, $2\alpha = 90°$ and d = 1 mm, as obtained by means of Ansys free mesh generation algorithm.

Figure 17: Non-dimensional ratio K^{*}_{FE} for (a) Ansys and (b) Abaqus FE codes. Results for mode I loading obtained by activating the full integration scheme and by adopting the principal stress averaging option of Fig. 15b.

Table 1: Values of notch parameters considered in the present work

Table 2: List of participants (alphabetic order) and FE codes.

Table 3: FE analyses of 2D problems (plane strain) under mode I loading.

Table 4: FE analyses of 2D problems (plane strain) under mode II loading.

Table 5: Results of Round Robin for mode I and mode II loadings. Mean values of non-dimensional ratios K^{*}_{FE} and K^{**}_{FE} and minimum mesh density ratio a/d for all considered FE codes.

Table 6: Options for principal stress averaging available in the considered FE codes.

Table 7: FE mesh patterns relevant to the case of Fig. 7c with a = 15 mm, $2\alpha = 90°$ and d = 1 mm, as obtained with different FE codes. Results in terms of peak stresses evaluated at the notch tip. Peak stress values obtained by adopting the *default options,* which have been employed to calibrate PSM, are highlighted.

Table 8: Peak stresses evaluated at the V-notch tip by using the mesh pattern of Fig. 16. Results based on nodal stresses (according to Eq. (10) and Fig. 13a). Peak stress values obtained by adopting *default options* are highlighted.

Table 9: Peak stresses evaluated at the V-notch tip by using the mesh pattern of Fig. 16. Results based on centroidal stresses (according to Eq. (11) and Fig. 13b). Peak stress values obtained by adopting *default options* are highlighted.

FIGURES

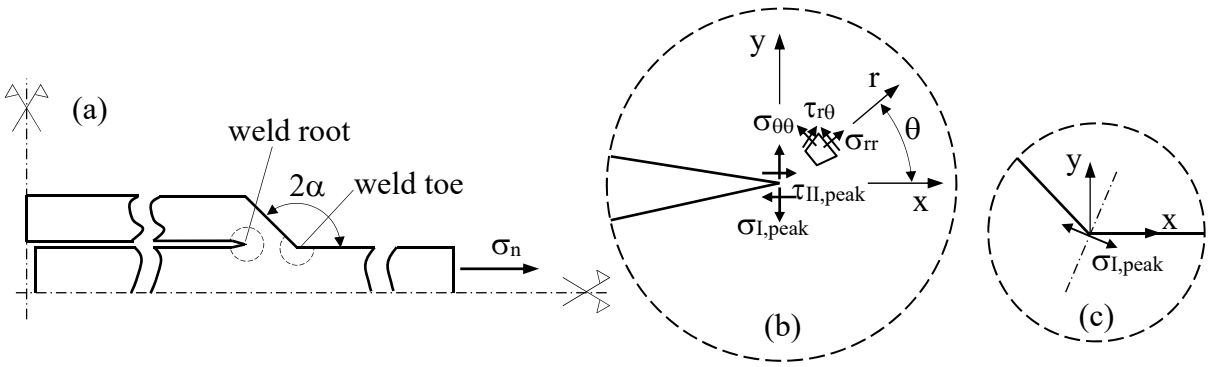

Figure 1: Sharp V-shaped notches in a welded joint (a) at the root ($2\alpha = 0°$) (b) and at the toe (2α typically equal to 135°) (c) sides. Definition of peak stresses $\sigma_{I,peak}$ and $\tau_{II,peak}$ evaluated at the weld toe and the weld root by means of a linear elastic finite element analysis.

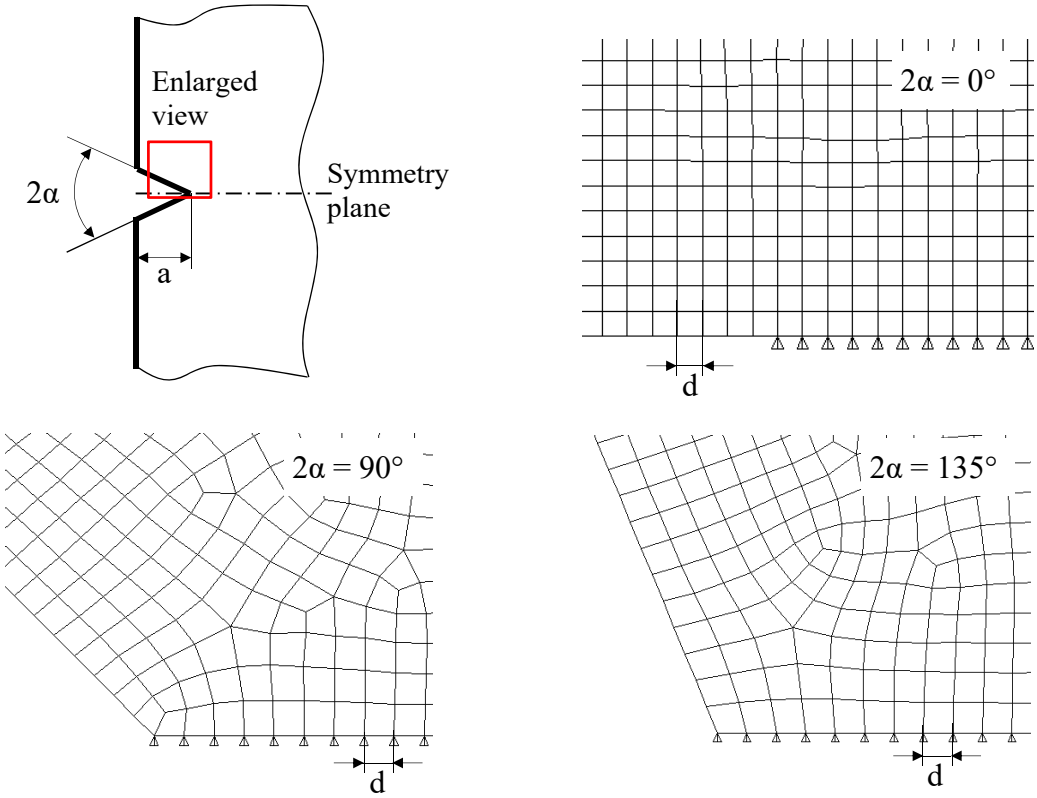

Figure 2: Mesh patterns according to the PSM[21,23]. Symmetry boundary conditions have been applied to the FE model.

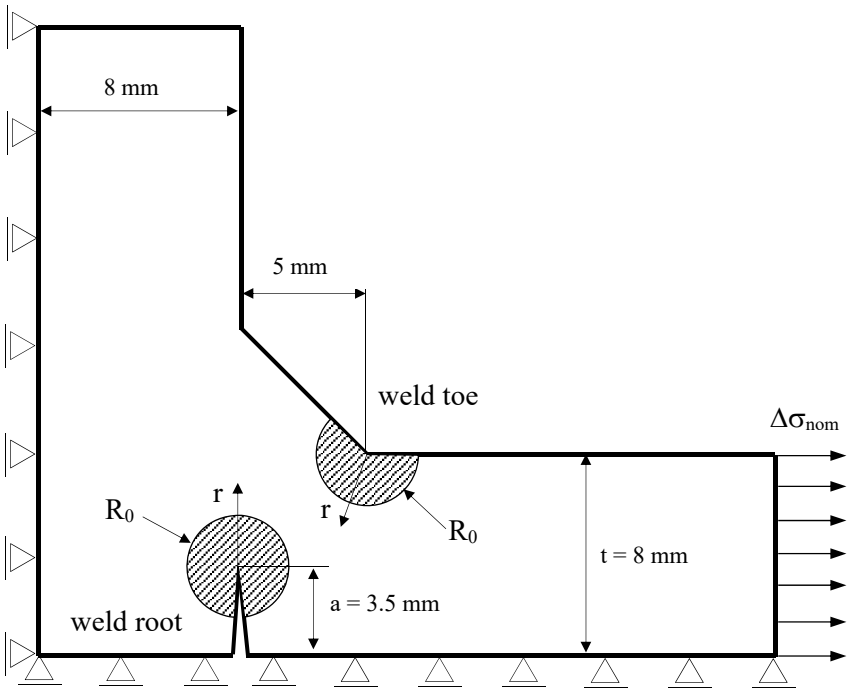

Figure 3: Geometry of the load-carrying steel weld joint tested in[31]. Control volumes for the averaged SED evaluation at the weld toe and the weld root sides.

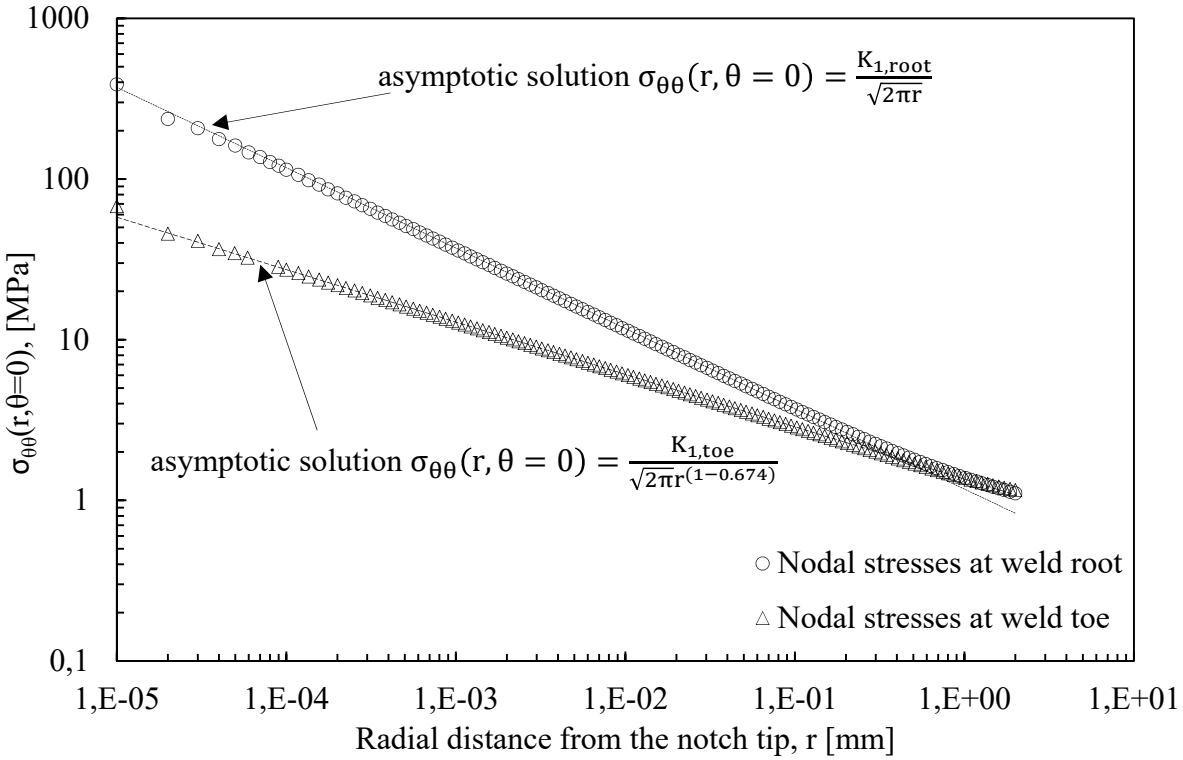

Figure 4: Singular, linear elastic stress fields at the weld toe and the weld root, obtained from very refined FE mesh patterns (minimum FE size $d_{min} \approx 10^{-5}$ mm) and comparison with the asymptotic solutions based on the relevant NSIF. The nominal applied stress $\Delta\sigma_{nom}$ is equal to 1 MPa.

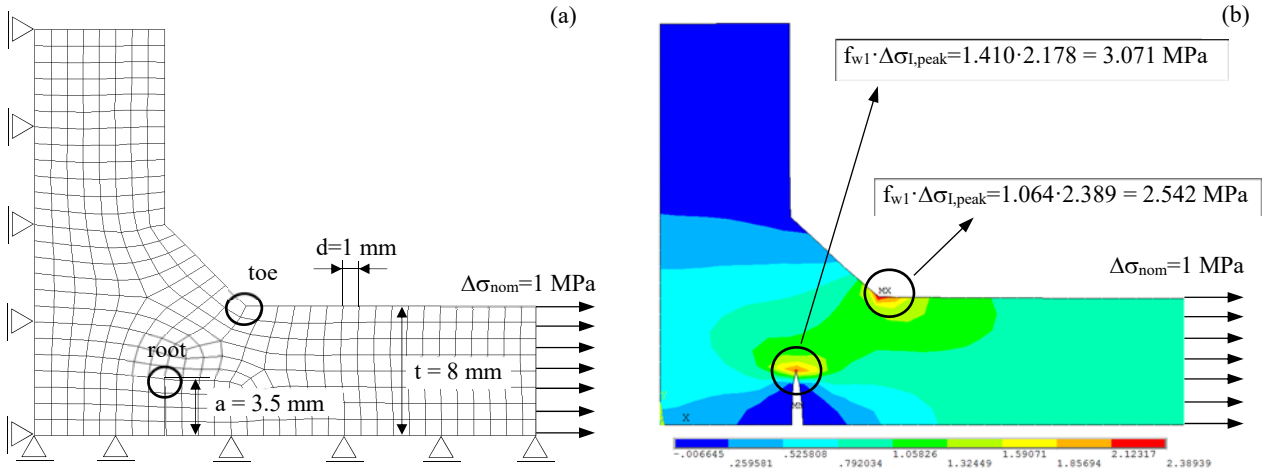

Figure 5: Application of the PSM to the fatigue strength assessment of a load-carrying arc-welded joint made of structural steel and tested in[31].

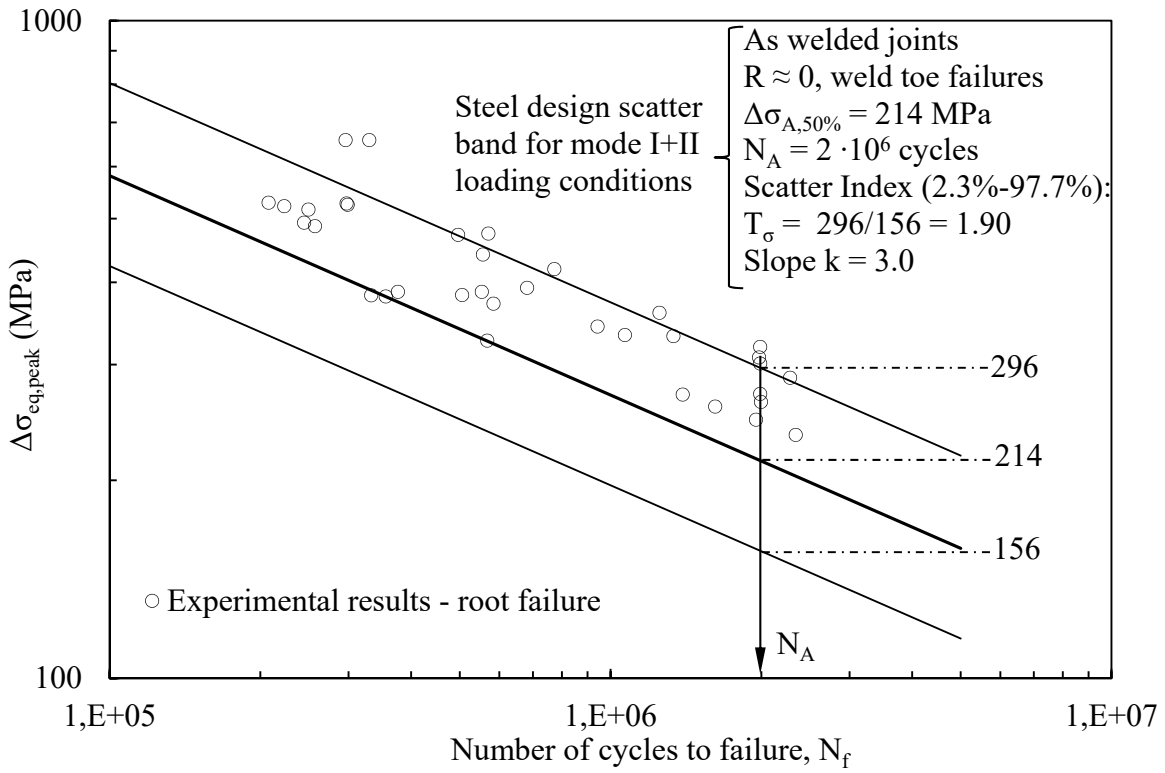

Figure 6: Fatigue assessment of load-carrying steel welded joints according to the PSM. Comparison between the fatigue design scatter band of the PSM[26] and experimental fatigue results from[31].

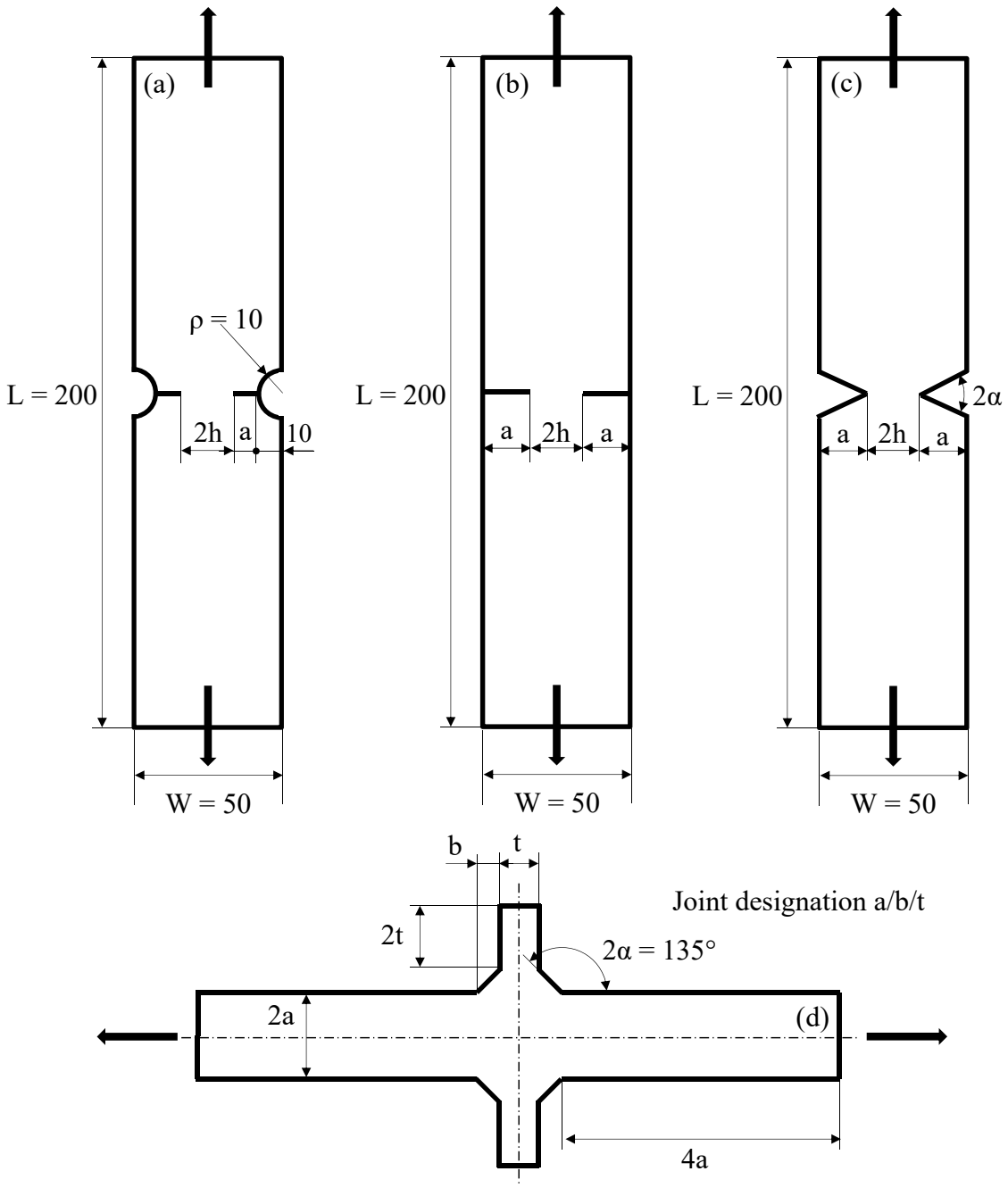

Figure 7: Geometries of 2D problems (plane strain) under mode I loading. Dimensions in [mm].

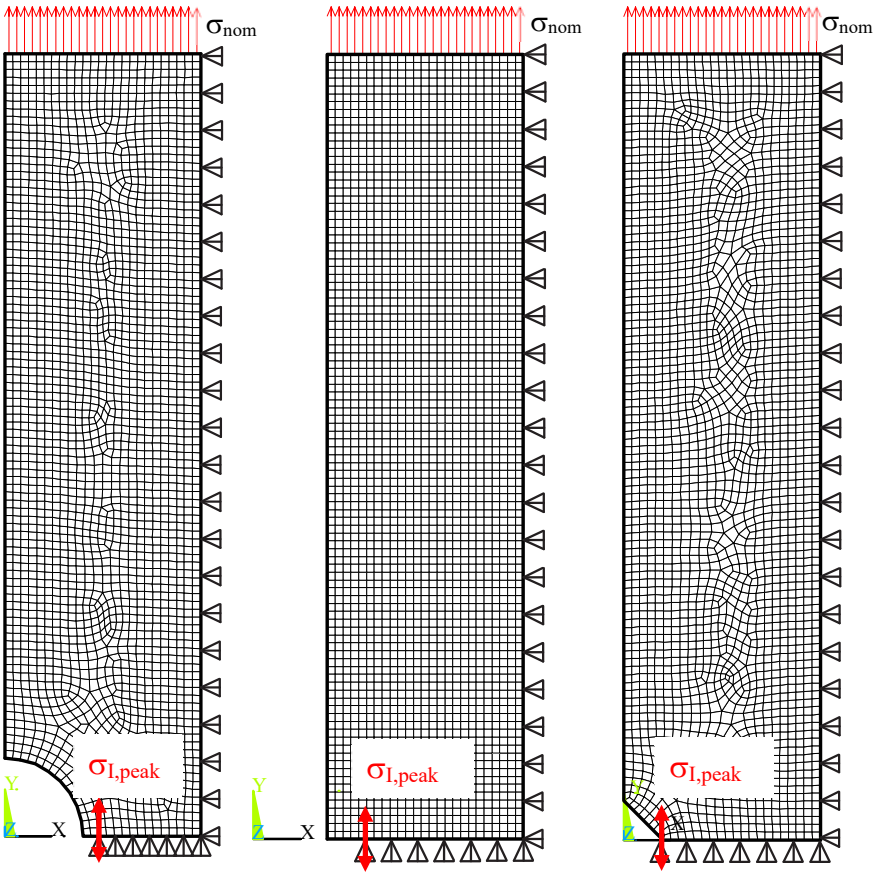

Fig. 7 (a) Fig. 7 (b) Fig. 7 (c)

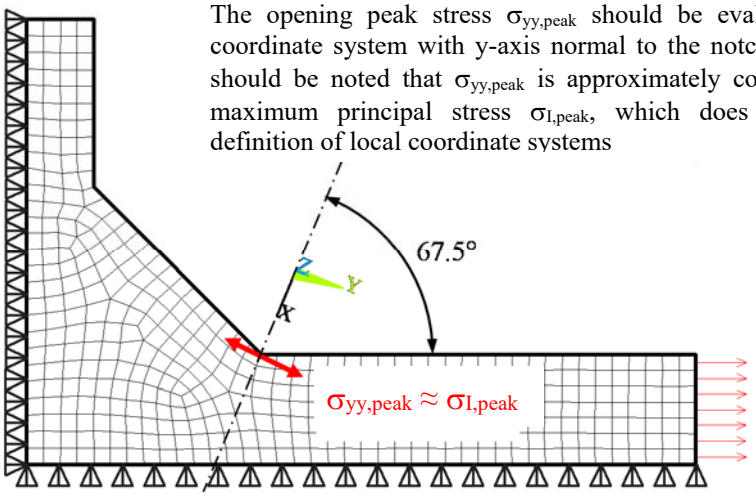

Fig. 7 (d)

Figure 8: FE mesh patterns and boundary conditions applied into the FE analyses of 2D problems (plane strain) under mode I loading. Geometries are reported in Fig. 7. FE patterns shown in the figure have been generated by using Ansys.

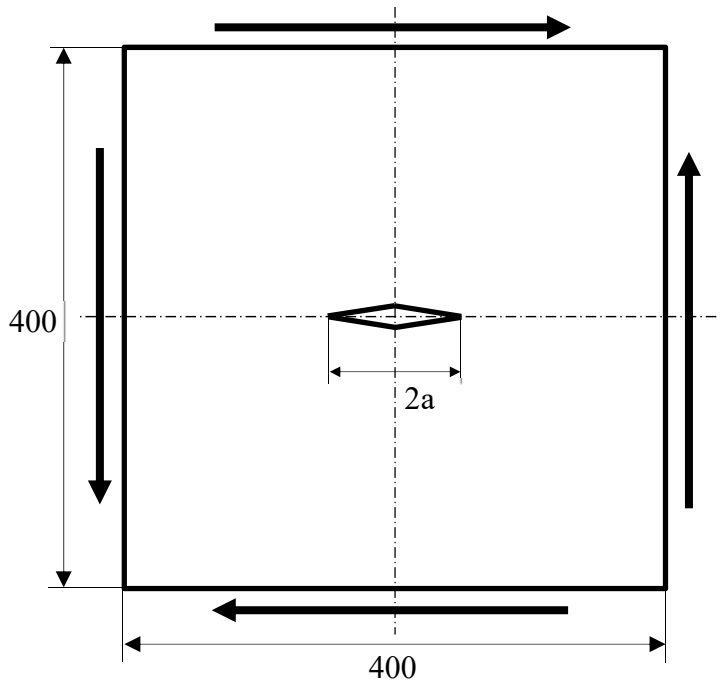

Figure 9: Geometry of 2D problems (plane strain) under mode II loading. Dimensions in [mm].

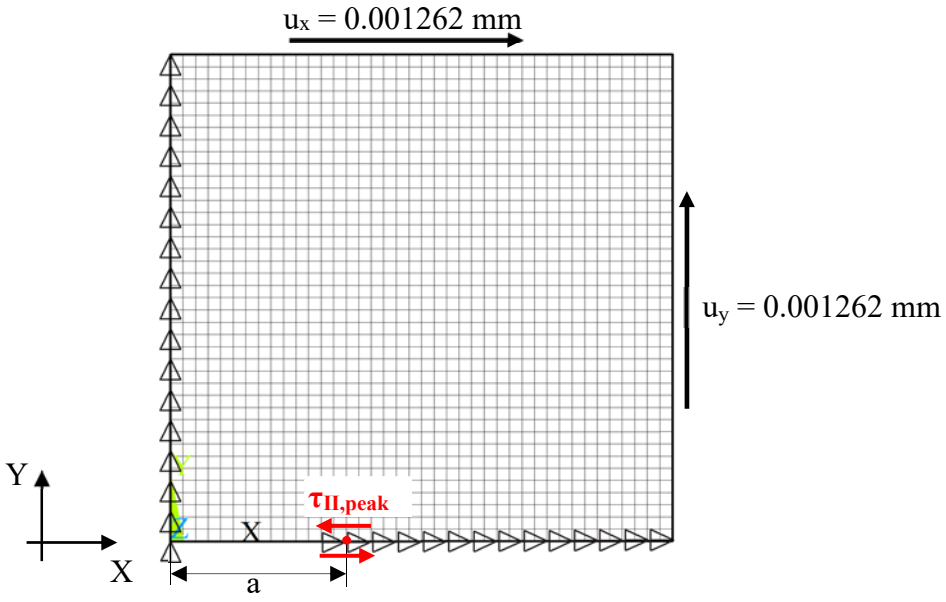

Figure 10: FE mesh pattern and boundary conditions applied into the FE analyses of 2D problems (plane strain) under mode II loading. Geometry is reported in Fig. 9. The FE pattern shown in the figure has been generated by using Ansys.

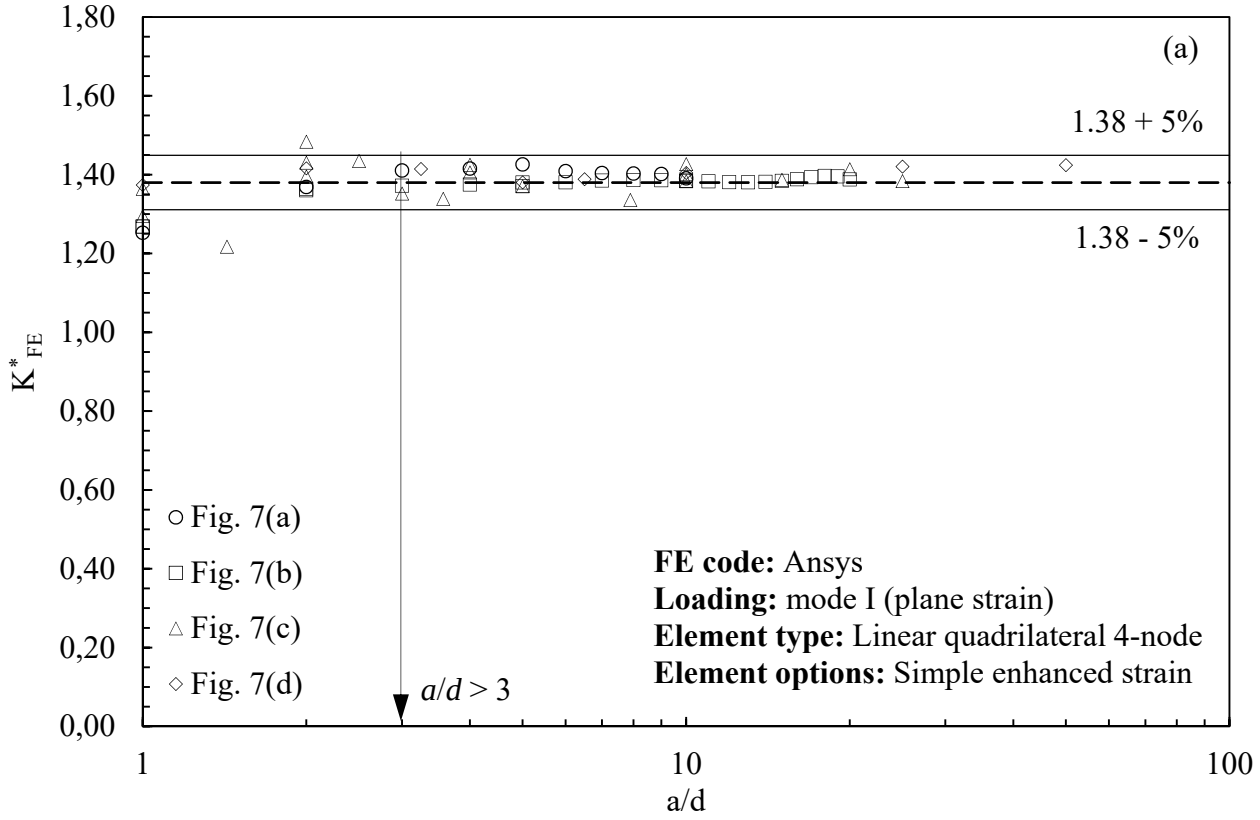
(a)
1.38 + 5%
1.38 - 5%
K^*_{FE}
○ Fig. 7(a)
□ Fig. 7(b)
△ Fig. 7(c)
◇ Fig. 7(d)
a/d > 3
FE code: Ansys
Loading: mode I (plane strain)
Element type: Linear quadrilateral 4-node
Element options: Simple enhanced strain
1,80
1,60
1,40
1,20
1,00
0,80
0,60
0,40
0,20
0,00
1
10
100
a/d

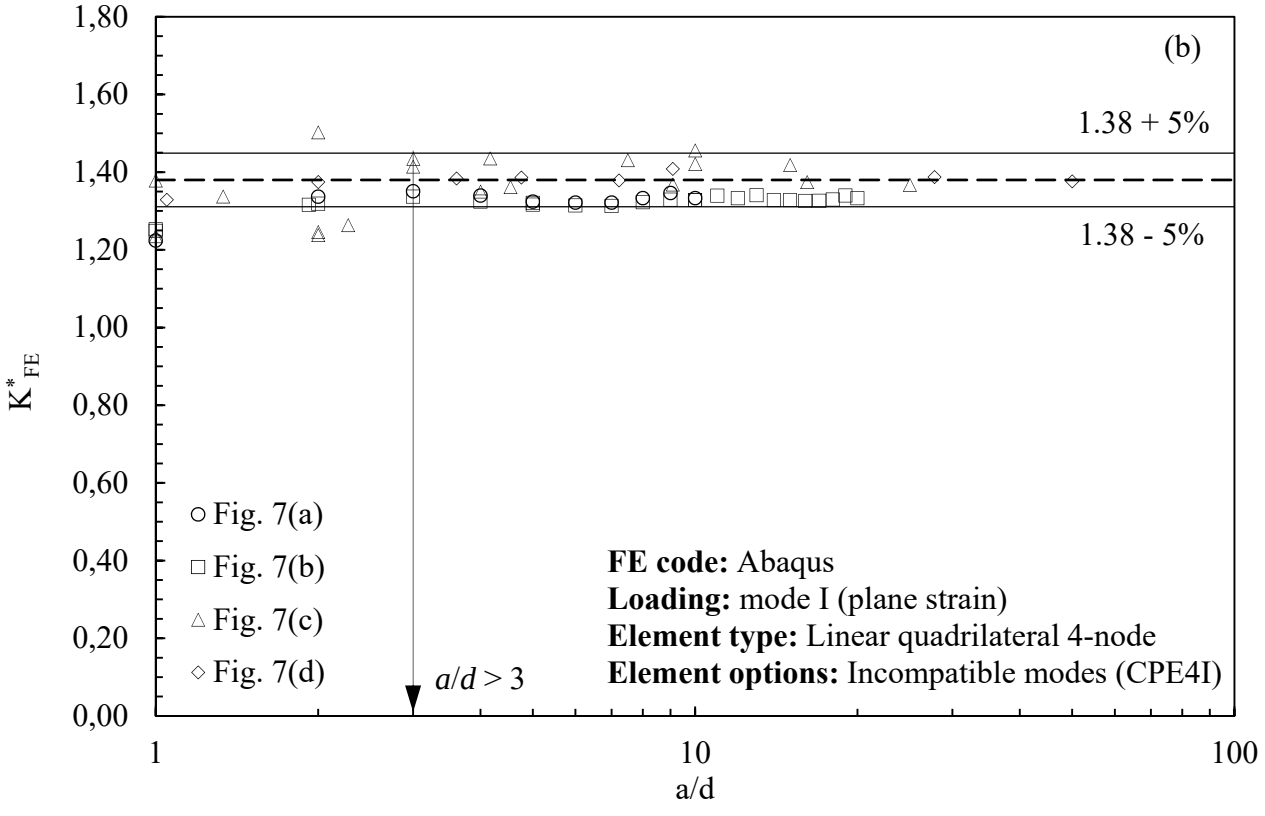
(b)
1.38 + 5%
1.38 - 5%
K^*_{FE}
○ Fig. 7(a)
□ Fig. 7(b)
△ Fig. 7(c)
◇ Fig. 7(d)
a/d > 3
FE code: Abaqus
Loading: mode I (plane strain)
Element type: Linear quadrilateral 4-node
Element options: Incompatible modes (CPE4I)
1,80
1,60
1,40
1,20
1,00
0,80
0,60
0,40
0,20
0,00
1
10
100
a/d

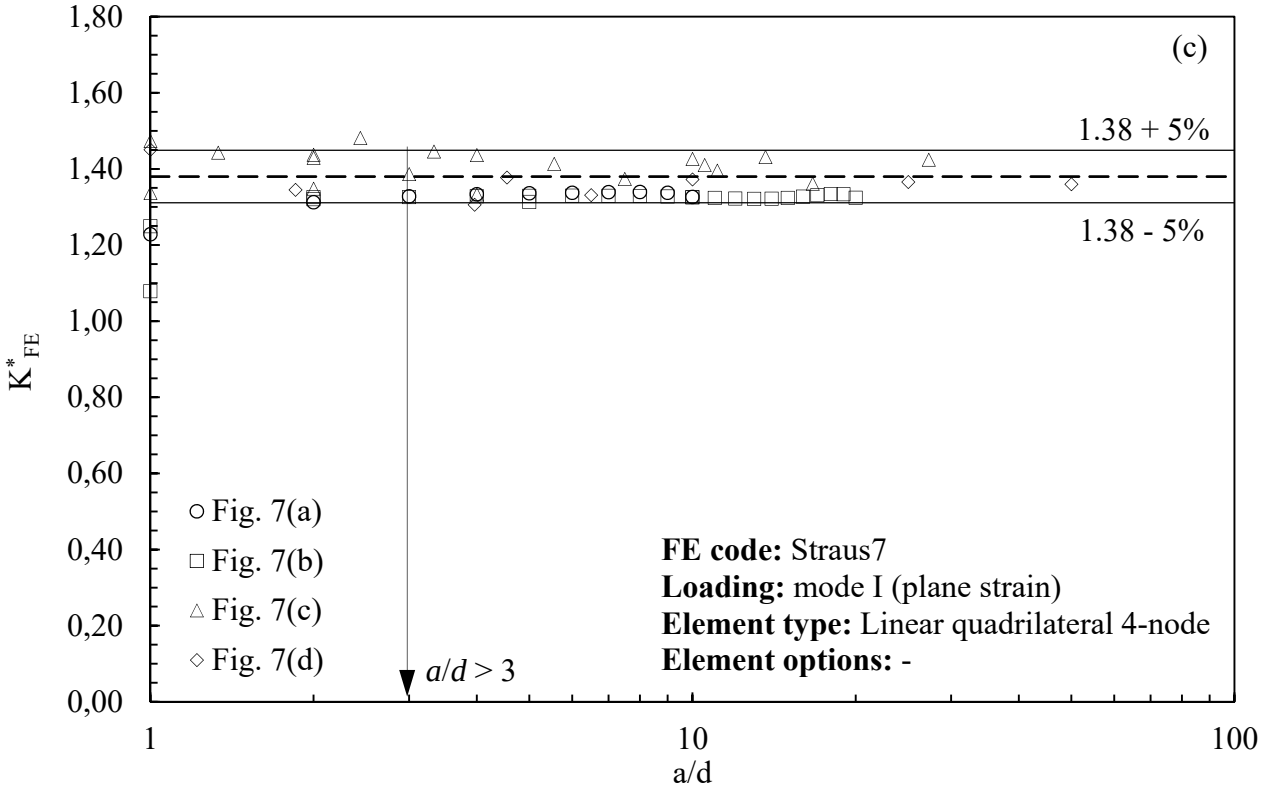
(c)
1.38 + 5%
1.38 - 5%
K^*_{FE}
1,80
1,60
1,40
1,20
1,00
0,80
0,60
0,40
0,20
0,00
○ Fig. 7(a)
□ Fig. 7(b)
△ Fig. 7(c)
◇ Fig. 7(d)
a/d > 3
FE code: Straus7
Loading: mode I (plane strain)
Element type: Linear quadrilateral 4-node
Element options: -
1
10
100
a/d

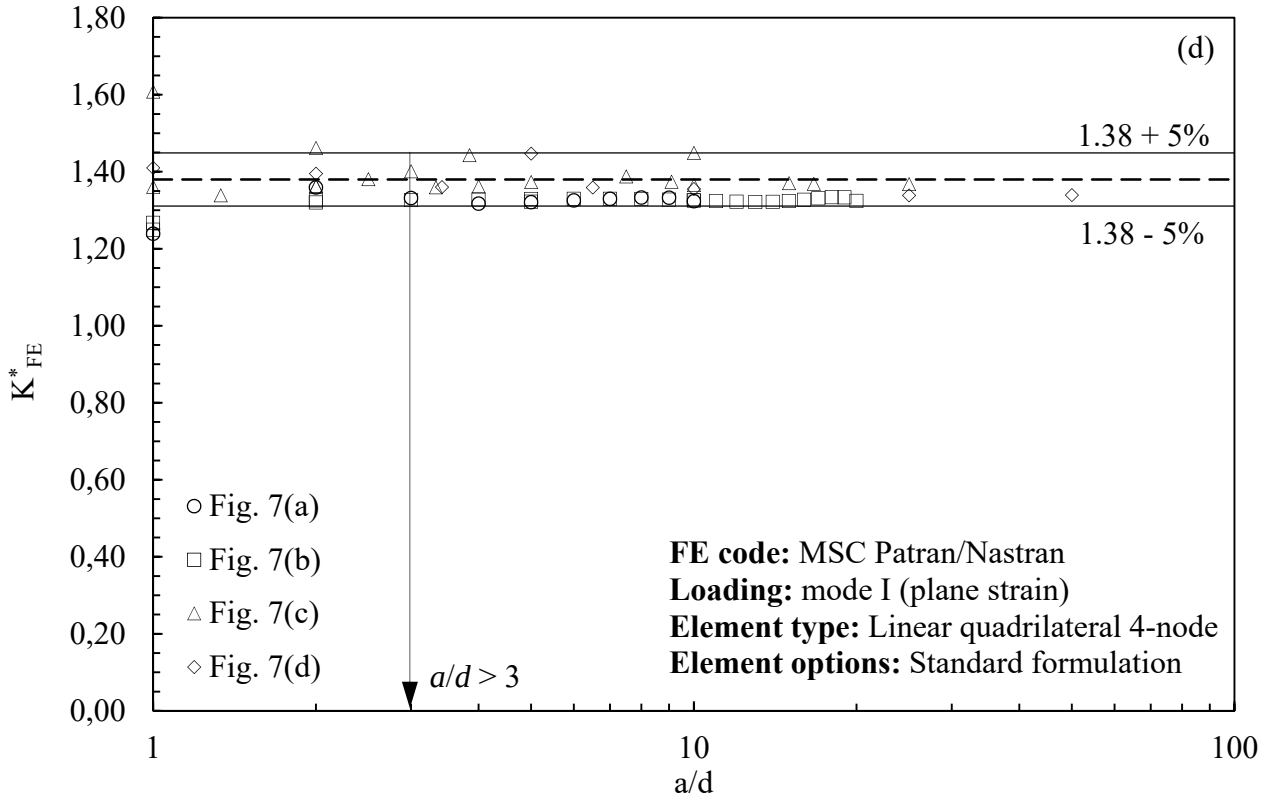
(d)
1.38 + 5%
1.38 - 5%
K^*_{FE}
1,80
1,60
1,40
1,20
1,00
0,80
0,60
0,40
0,20
0,00
○ Fig. 7(a)
□ Fig. 7(b)
△ Fig. 7(c)
◇ Fig. 7(d)
a/d > 3
FE code: MSC Patran/Nastran
Loading: mode I (plane strain)
Element type: Linear quadrilateral 4-node
Element options: Standard formulation
1
10
100
a/d

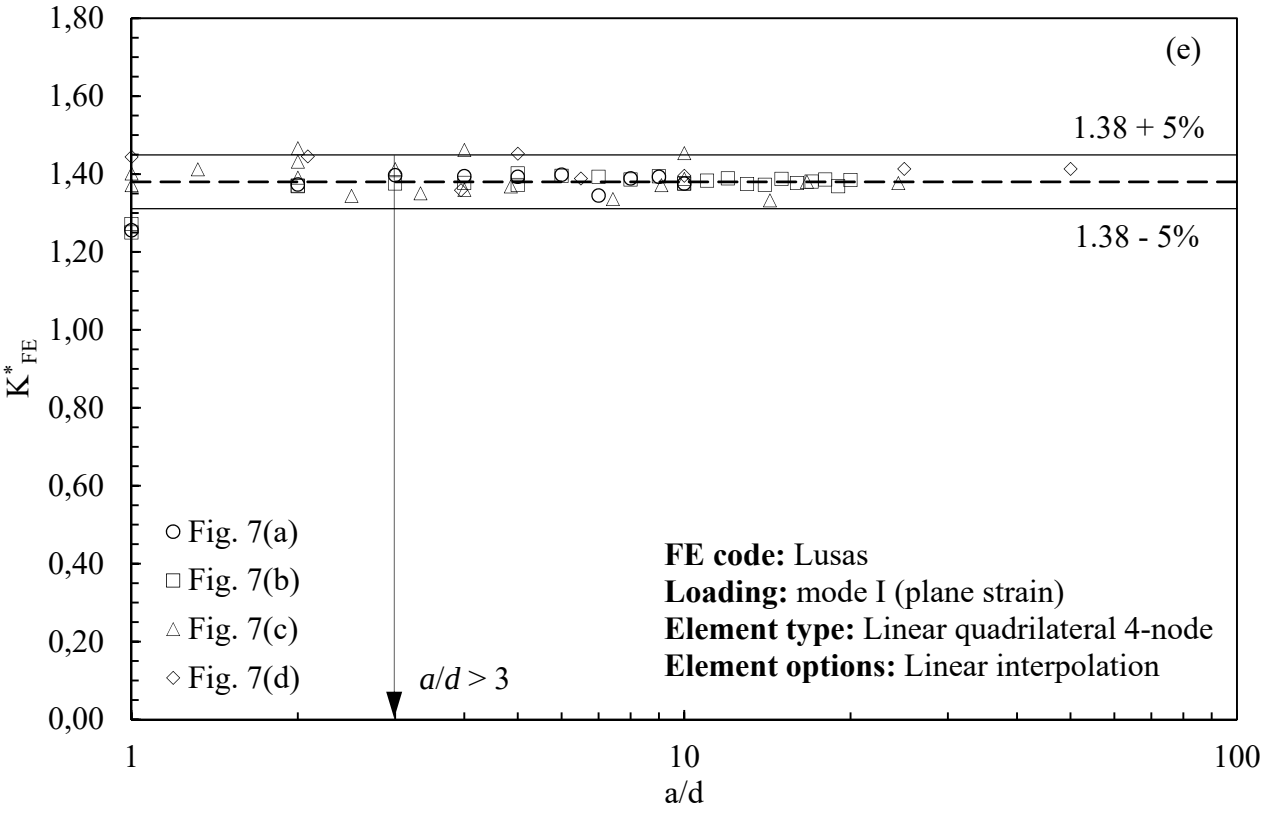
(e)
1.38 + 5%
1.38 - 5%
K*FE
1,80
1,60
1,40
1,20
1,00
0,80
0,60
0,40
0,20
0,00
Fig. 7(a)
Fig. 7(b)
Fig. 7(c)
Fig. 7(d)
a/d > 3
FE code: Lusas
Loading: mode I (plane strain)
Element type: Linear quadrilateral 4-node
Element options: Linear interpolation
1
10
100
a/d

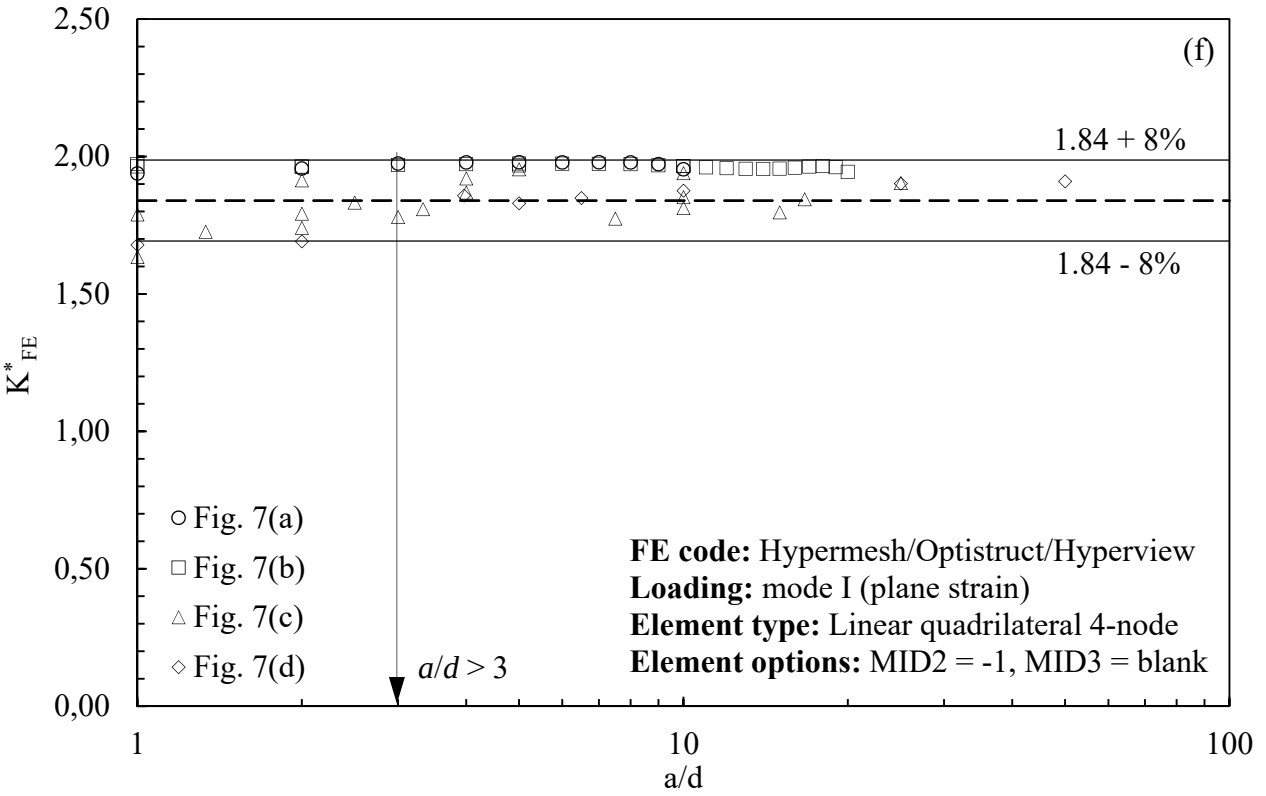
(f)
1.84 + 8%
1.84 - 8%
K*FE
2,50
2,00
1,50
1,00
0,50
0,00
Fig. 7(a)
Fig. 7(b)
Fig. 7(c)
Fig. 7(d)
a/d > 3
FE code: Hypermesh/Optistruct/Hyperview
Loading: mode I (plane strain)
Element type: Linear quadrilateral 4-node
Element options: MID2 = -1, MID3 = blank
1
10
100
a/d

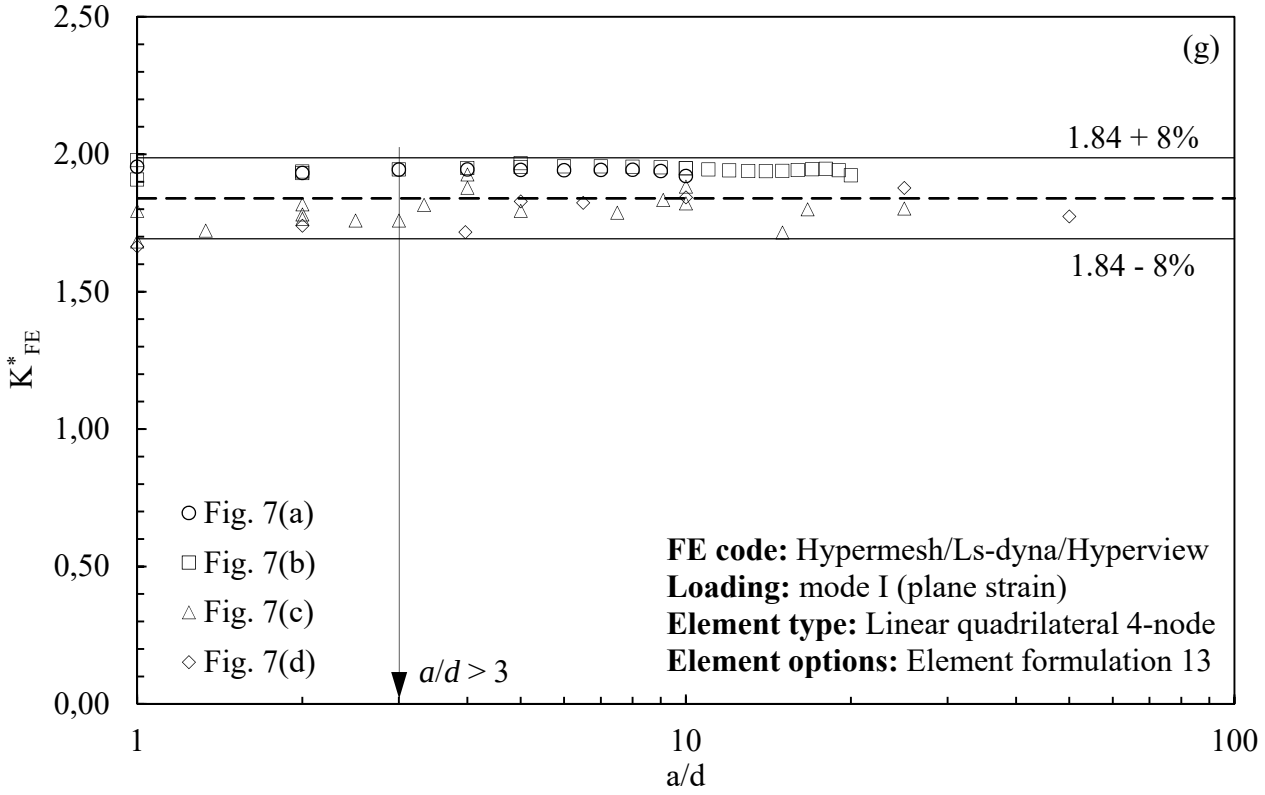

Figure 11: Results of Round Robin for mode I loading: non-dimensional ratio K^{*}_{FE} for each FE code.

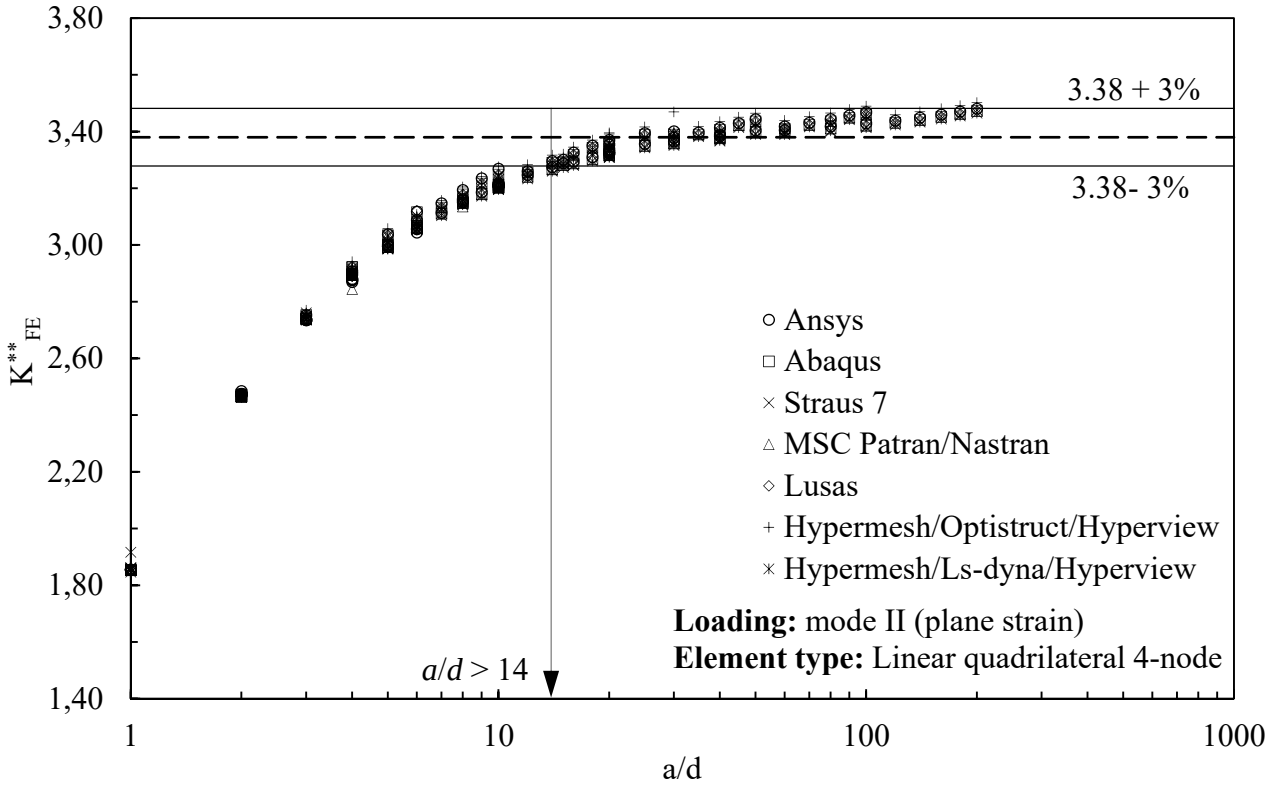

Figure 12: Results of Round Robin for mode II loading: non-dimensional ratio K^{**}_{FE} for all considered FE codes.

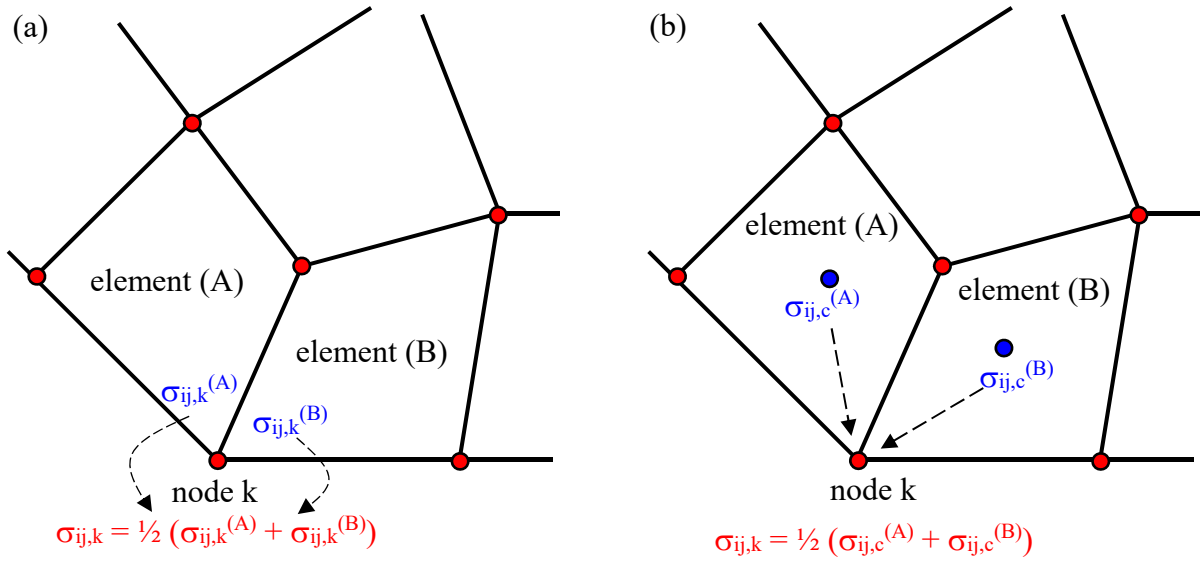

Figure 13: Stress extrapolation at the nodes based on (a) nodal stresses or (b) centroidal stresses.

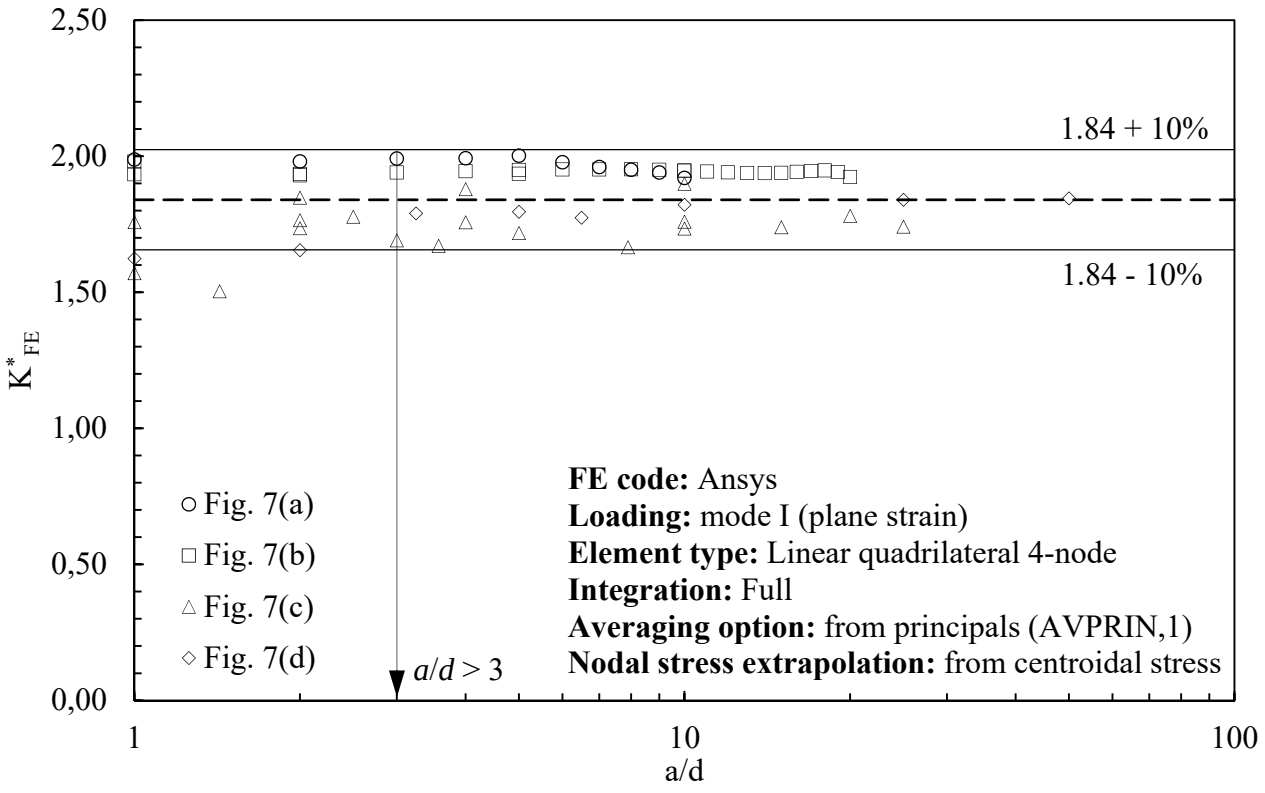

Figure 14: Non-dimensional ratio K^*_{FE} for Ansys FE code. Results for mode I loading based on centroidal stresses (according to Fig. 13b).

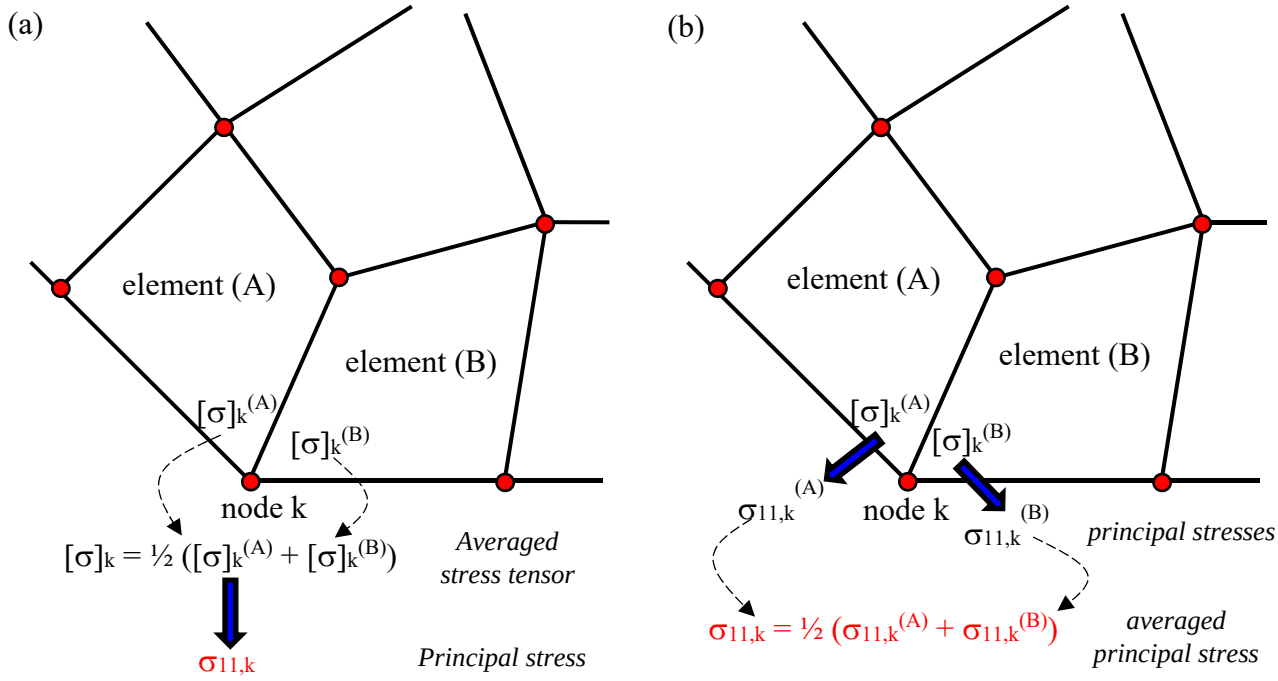

Figure 15: Principal stress averaging options. (a) Principal stresses from average stress tensor. (b) Principal stresses from element principal stresses.

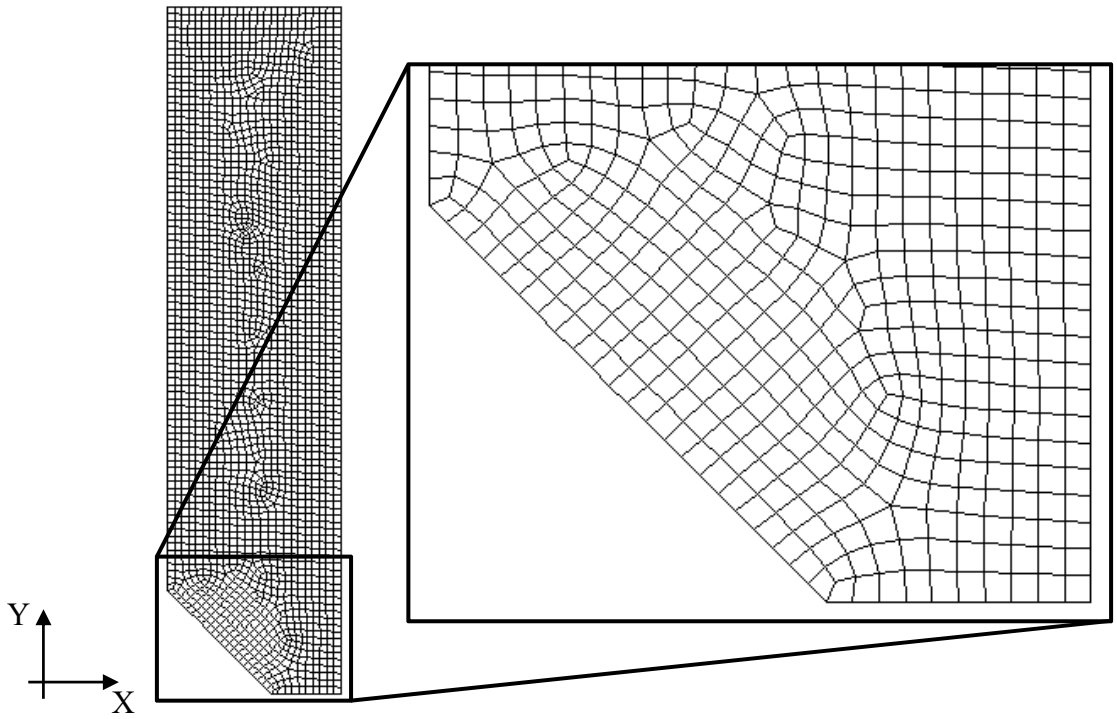

Figure 16: FE mesh pattern relevant to case 7c with a = 15 mm, 2α = 90° and d = 1 mm, as obtained by means of Ansys free mesh generation algorithm.

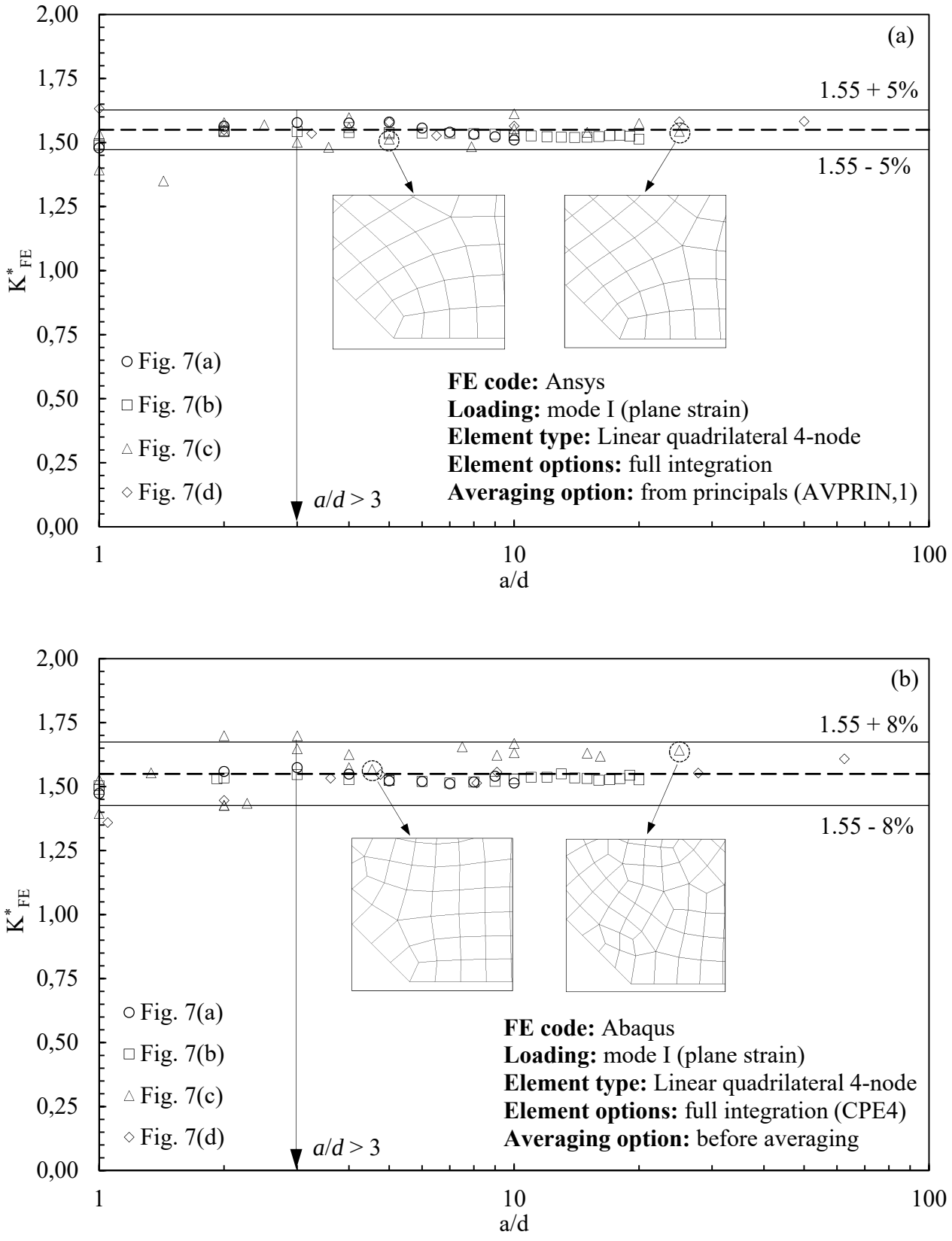

Figure 17: Non-dimensional ratio K^*_{FE} for (a) Ansys and (b) Abaqus FE codes. Results for mode I loading obtained by activating the full integration scheme and by adopting the principal stress averaging option of Fig. 15b.

TABLES

Table 1: Values of notch parameters considered in the present work

2α (deg)	λ_1	e_1^*	λ_2	e_2^*
0	0.500	0.133	0.500	0.340
90	0.544	0.145		
135	0.674	0.118		

*: values from[7]

Table 2: List of participants (alphabetic order) and FE codes.

Universities (alphabetic order)	**FE codes (alphabetic order)**
Bologna (UNIBO)	Ansys 16 and 17
Genova (UNIGE)	Abaqus 6.13 and 6.14
Messina (UNIME)	Hypermesh 14*/Optistruct 14 implicit/Hyperview 14**
Modena and Reggio Emilia (UNIMORE)	Hypermesh 13*/Ls-Dyna R7.1.3 implicit/Hyperview 13**
Padova (UNIPD)	Lusas 14.6-2
Palermo (UNIPA)	MSC Patran/Nastran 2014 and 2016
Parma (UNIPR)	Straus 7 R.2.4.6
Pisa (UNIPI)	
Torino (POLITO)	
Trento (UNITN)	

*: pre-processor; **: post-processor

Table 3: FE analyses of 2D problems (plane strain) under mode I loading.

Analysed geometries						
Figure	**a [mm]**	**d [mm]**	**2α [°]**	**b [mm]**	**t [mm]**	**Number of analyses****
7(a)	1, 2,…,9, 10	1	0	-	-	10
7(b)	1, 2,…,19, 20	1	0	-	-	20
7(b)	10	1, 2, 5, 10	0	-	-	4
7(c)	10	1, 2.5, 5, 10	135	-	-	4
7(c)	5	0.5, 1, 2, 2.5, 5	90	-	-	5
7(c)	10	0.6, 1, 2.5, 3, 5, 7.5	90	-	-	6
7(c)	15	0.6, 1, 2, 5	90	-	-	4
7(d)	6.5	1, 1.64, 6.5	135	10	8	3
7(d)	50	1, 2, 5, 10, 25	135	50	16	5

**: total number of analyses: 61

Table 4: FE analyses of 2D problems (plane strain) under mode II loading.

Analysed geometries			
a [mm]	**d [mm]**	**2α [°]**	**Number of analyses ****
1	0.5, 1	0	2
2	0.5, 1, 2	0	3
3	0.5, 1, 3	0	3
4	0.5, 1, 2, 4	0	4
5	0.5, 1, 5	0	3
6	0.5, 1, 2, 3	0	4
7	0.5, 1	0	2
8	0.5, 1, 2, 4	0	4
9	0.5, 1, 3	0	3
10	0.5, 1, 2, 5, 10	0	5
20	0.5, 1, 2, 4, 5, 10	0	6
30	0.5, 1, 2, 3, 5, 10, 15	0	7
40	0.5, 1, 2, 4, 5, 10, 20	0	7
50	0.5, 1, 2, 5, 10	0	5
60	0.5, 1, 2, 3, 4, 5, 10, 15, 20	0	9
70	0.5, 1, 2, 5, 10	0	5
80	0.5, 1, 2, 4, 5, 10, 20	0	7
90	0.5, 1, 2, 3, 5, 10, 15	0	7
100	0.5, 1, 2, 4, 5, 10, 20	0	7

**: total number of analyses: 93

Table 5: Results of Round Robin for mode I and mode II loadings. Mean values of non-dimensional ratios K^{*}_{FE} and K^{**}_{FE} and minimum mesh density ratio *a/d* for all considered FE codes.

Software	**Element /n° nodes**	**Integration/ Gauss points**	**Element shape**	**Mesh generation technique**	K^{*}_{FE} (Eq. (5))			K^{**}_{FE} (Eq. (6))		
					value	Opening angle	Min *a/d*	value	Opening angle	Min *a/d*
Ansys 16 and 17	PLANE 182/ 4 node	Simple enhanced strain/ 2x2	Quadrangular	Free-mesh, global element size *d*	1.38±5%	0°≤2α≤135°	3	3.38±3%	0°	14
Abaqus 6.13 and 6.14	CPE4I/ 4-node	Incompatible modes/ 2x2	Quadrangular		1.38±5%	0°≤2α≤135°	3	3.38±3%	0°	14
Straus 7 R2.4.6	QUAD 4/ 4-node	Incompatible modes/ 2x2	Quadrangular		1.38±5%	0°≤2α≤135°	3	3.38±3%	0°	14
MSC Patran/ Nastran 2014 and 2016	CQUAD4/ 4-node	Standard formulation/ 2x2	Quadrangular		1.38±5%	0°≤2α≤135°	3	3.38±3%	0°	14
Lusas 14.6-2	QPN4M/ 4-node	Full with Enh. Strain/ 2x2	Quadrangular		1.38±5%	0°≤2α≤135°	3	3.38±3%[#]	0°	14
Hypermesh 14/ Optistruct 14 implicit/ Hyperview 14	Shell 4-node/ CQUAD4	*n.a.*, 2x2	Quadrangular		1.84±8%	0°≤2α≤135°	3	3.38±3%	0°	14
Hypermesh 13/ LSTC Ls-Dyna R7.1.3 implicit/ Hyperview 13	Shell 4-node/ Element formulation 13	*n.a.*, 2x2	Quadrangular		1.84±8%	0°≤2α≤135°	3	3.38±3%	0°	14

calibration obtained by adopting mapped-mesh with “global element size” *d*

Table 6: Options for principal stress averaging available in the considered FE codes.

FE Software	**Averaging option (a)**	**Averaging option (b)**
Ansys	AVPRIN,0 or "from components" (*default*)	AVPRIN,1 or "from principals"
Abaqus	"compute scalars after averaging"	"compute scalars before averaging" (*default*)
Straus 7	*not available*	Node average: "Always" (*default*)
MSC Patran/Nastran	Average/Derive	Derive/Average (*default*)
Lusas	Averaged nodal (*default*)	*not available*
Hyperview*	Averaging method: "Advanced"	Averaging method: "Simple" (*default*)

***** Post-processor adopted to calibrate both Optistruct and Ls-Dyna

Table 7: FE mesh patterns relevant to the case of Fig. 7c with a = 15 mm, $2\alpha = 90°$ and d = 1 mm, as obtained with different FE codes. Results in terms of peak stresses evaluated at the notch tip. Peak stress values obtained by adopting the *default options,* which have been employed to calibrate PSM, are highlighted.

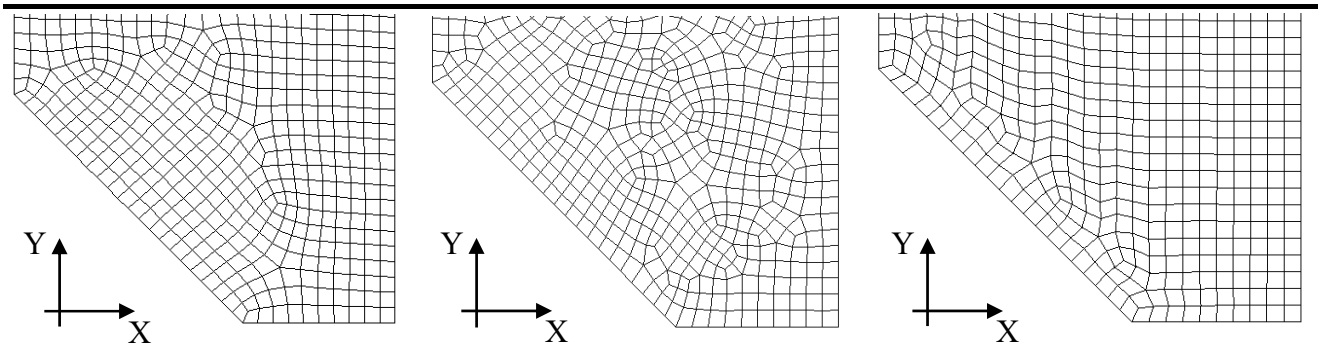

Ansys	**Abaqus**	**MSC Patran/Natran**
$\sigma_{yy,peak}/\sigma_{nom}$ = 6.185	$\sigma_{yy,peak}/\sigma_{nom}$ = 5.833	$\sigma_{yy,peak}/\sigma_{nom}$ = 6.092
$\sigma_{I,peak}/\sigma_{nom}$ = 6.309 (*default*) Averaging option (a)	$\sigma_{I,peak}/\sigma_{nom}$ = 5.918 Averaging option (a)	$\sigma_{I,peak}/\sigma_{nom}$ = 6.183 Averaging option (a)
$\sigma_{I,peak}/\sigma_{nom}$ = 6.514 Averaging option (b)	$\sigma_{I,peak}/\sigma_{nom}$ = 6.093 (*default*) Averaging option (b)	$\sigma_{I,peak}/\sigma_{nom}$ = 6.386 (*default*) Averaging option (b)

Table 8: Peak stresses evaluated at the V-notch tip by using the mesh pattern of Fig. 16. Results based on nodal stresses (according to Eq. (10) and Fig. 13a). Peak stress values obtained by adopting *default options* are highlighted.

Software	**Ansys**			**Abaqus**			**Straus 7**	**Patran/ Nastran**	**Lusas**
Element type	Plane 182			CPE4I	CPE4H	CPE4	QUAD4	CQUAD4	QPN4M
Integration	Simple Enh. strain	Enh. strain	Full	Incomp. modes	Hybrid	Full	Incomp. modes	Standard formulation	Full with Enh. strain
Gauss points	2x2			2x2			2x2	2x2	2x2
Stress state	Plane strain			Plane strain			Plane strain	Plane strain	Plane strain
$\sigma_{yy,peak}/\sigma_{nom}$	6.185	6.260	5.361	6.260	5.361	5.361	6.120	6.185	6.227
$\sigma_{I,peak}/\sigma_{nom}$ **Averaging option (a)**	6.309 *(default)*	6.386	5.445	6.386	5.445	5.445	*n.a.*	6.309	6.312 *(default)*
$\sigma_{I,peak}/\sigma_{nom}$ **Averaging option (b)**	6.514	6.590	5.683	6.590 *(default)*	5.683	5.683	6.445 *(default)*	6.514 *(default)*	6.492

Table 9: Peak stresses evaluated at the V-notch tip by using the mesh pattern of Fig. 16. Results based on centroidal stresses (according to Eq. (11) and Fig. 13b). Peak stress values obtained by adopting *default options* are highlighted.

Software	**Hypermesh/Ls-Dyna/ Hyperview**	**Hypermesh/Optistruct/ Hyperview**	**Ansys**			**Straus 7**
Element type	Shell 4 node, Element formulation 13	Shell CQUAD4	Plane 182			QUAD4
Integration	*n.a.*	*n.a.*	Simple Enh. strain	Enh. strain	Full	Incomp. modes
Gauss points	2x2	2x2	2x2			2x2
Stress state	Plane strain	Plane strain	Plane strain			Plane strain
$\sigma_{yy,peak}/\sigma_{nom}$	4.770	4.743	4.720	4.720	4.781	4.718
$\sigma_{I,peak}/\sigma_{nom}$ **Averaging option (a)**	4.898	4.874	4.840	4.840	4.910	*n.a.*
$\sigma_{I,peak}/\sigma_{nom}$ **Averaging option (b)**	5.019 *(default)*	5.003 *(default)*	4.962	4.962	5.031	4.965